Pouch Motors: Printable Pneumatic Actuators for Foldable Robotics

by

Xu Sun

B.S. in Mechanical Engineering - Design Innovation and Society,
Rensselaer Polytechnic Institute (2013)

Submitted to the Department of Mechanical Engineering
in partial fulfillment of the requirements for the degree of

Master of Science in Mechanical Engineering

at the

MASSACHUSETTS INSTITUTE OF TECHNOLOGY

June 2015

Signature redacted

Author .....
Department of Mechanical Engineering
May 18, 2015

Signature redacted

Certified by .....
Sangbae Kim
Associate Professor, Department of Mechanical Engineering
Thesis Supervisor

Signature redacted

Accepted by .....
David E. Hardt
Ralph E. and Eloise F. Cross Professor in Manufacturing
Graduate Officer, Department of Mechanical Engineering

Pouch Motors: Printable Pneumatic Actuators for Foldable Robotics

by

Xu Sun

Submitted to the Department of Mechanical Engineering
on May 18, 2015, in partial fulfillment of the
requirements for the degree of
Master of Science in Mechanical Engineering

Abstract

We envision future electro-mechanical devices can be printed on planer structures and folded autonomously for robotic applications. This thesis project is devoted for the development of self-folding and actuation of such robots, with a novel actuator called pouch motors. Pouch motors is a family of printable pneumatic actuators in the pouch form that drives motion with inflations and deflations. It is customizable in design, inexpensive to fabricate and planer in nature, making it ideal for origami inspired robots. In the first half of this thesis, Pouch motor's actuation mechanisms with theoretical and experimental assessments are introduced. Design and fabrication work flows are described. In the second half of the thesis, different configurations of pouch motors are presented not only for robot self-folding, but also for applications in human computer interaction. The thesis highlights the robotic garden project as a representative example, bringing a discussion of future development.

Thesis Supervisor: Sangbae Kim
Title: Associate Professor, Department of Mechanical Engineering

Acknowledgments

My deepest gratitude goes to my advisor Professor Sangbae Kim. Robotics was all new to me when I just joined Biomimetic Robotics Lab (BRL). Thank you for introducing me to this area, and putting your belief in me with your tireless guidance.

I also would like to express my appreciation to Professor Daniela Rus from MIT Computer Science and Artificial Intelligence Lab and Professor Rob Wood from Harvard Microrobotics Lab for providing advice on foldable robotics research.

My research project wouldn't be possible without the prior work from Dr. Ryuma Niiyama. I sincerely appreciate your guidance while we were working together and your extensive support when you left. The same goes to Dr. Sam Felton and other fellow researchers. It was such a great experience working with you all. I thank you for your knowledge and inspiration.

I'd like to thank my fellow BRL lab mates for having me, for our friendship, for our constant exploration trips for better taste wings in Boston, or simply hanging out for a drink after a long day's work at night.

Lastly but most importantly, I'd like to thank my parents. Your love is a constant source of strength, support and encouragement throughout my life.

This thesis work is based on Dr. Ryuma Niiyama's introduction of the pouch motors [26]. As a part of *An Expedition in Computing for Compiling Printable Programmable Machines*, this project is funded by National Science Foundation. The grant numbers are: 1240383 and 1138967.

Contents

List of Figures

List of Tables

Chapter 1

Introduction

People generally perceive robots as rigid structures holding electronic boards and wires. They are assembled with multiple electromechanical components through laborious manufacturing processes. This nature of complexity in manufacturing and design, time and cost, drastically limits robot development and commercialization [27].

Instead of traditional fabrication means, in *An Expedition in Computing for Compiling Printable Programmable Machines*, we approach this challenge by "printing" and "folding". This introduces a new class of robots that are folded up from sheet materials and look like origamis.

1.1 Towards Origami Inspired Robots

1.1.1 Fabrication by Printing

Recent advances in printing technologies support the development of origami inspired foldable robots. Shape Deposition Manufacturing (SDM) processes such as 3D printing, allow customized structures to be made in house on demand. Pick-and-place processes open up possibilities of integration of sensors and actuators into layered deposited structures [2,26].

In material science, HCI and other domains, researchers have developed technologies to print circuits [17] including batteries [33], optics [37] and polymer transistors [27,32]. Other researchers have combined those developments into robotics, using robot bodies as

substrates to hold its electronics components [29].

1.1.2 Fabrication by Folding

Bending has long been used in sheet metal processing. Researchers from robotics field recognize this fabrication process as a simple mean to construct robotic structures, and developed layered composite materials for folding and complaint joints [15, 27, 38].

To automate folding process, Hawkes et al. embedded Shape Memorable Alloy (SMA) into the composite material. This "programmable matter" has a predefined corrugate shape, which it will autonomously fold into from flat with a thermal signal [14]. This idea of self reconfigurable folding was later on further developed and become the foundation of what is called robot "self-folding".

Self-folding is an autonomous process [10] as it allows 3D structures to form without human manipulation [22]. Beside using shape memorable material such as SMA, other self-folding mechanisms exploit magnetism [3, 16], light [20], or material expansion [13]. These methods are usually triggered from external stimuli, posing limitations of the folding environment. Other common shortcomings include not strong enough to provide a torque to fold bigger structures [34].

Self-folding methods using shape memorable materials including SMA and Shape Memorable Polymers (SMP) are prevalent. Like SMA in "programmable matter", SMP can also be embedded in a self-folding laminate [10, 36]. SMP shrinks upon heating, curving the laminate at pre-cut hinge. Robotic structures self-folded with this method includes [1, 8, 9, 11, 31]. The limitation of SMP self-folding falls on requiring a vast amount of energy for heating, and yet the folded angles are not very accurate [34].

1.2 Towards Printable Actuators

Current fabrication by printing and folding provides viable solutions for making robots. However, there still lacks a printable actuators capable of controllable and continuous motions. Traditional actuators are electromagnetic motors that contain magnetic materials in a specific composition that is not compatible with printable processes. SDM is a feasible

candidate to make such motors [2, 6], but it requires customized parts and is rather complex to setup. They are also too heavy for folded robots, as it raises countering torque at the folding joint. Other commonly used actuators such as electrostatic and piezoelectric actuators are simpler to construct [7], but they are generally weak at generating forces.

In comparison, fluidic cylinders are mechanically simpler [26]. A traditional fluidic cylinder contains a moving piston, but recent development of fluidic actuators in robotics, such as Pneumatic Artificial Muscle (PAM), utilizes the shape change of a soft "air bag". This leads to a promising direction for the development of a printable actuator.

1.2.1 Advances in Fluidic Actuators

PAM is a family of the fluidic actuators that utilize the contraction of the air container upon inflation to drive linear motions, without any moving parts. Like many other types of PAM and its later improved versions, the popular original braided muscle [4] is essentially a sleeve containing a bladder with end fittings. Although the soft body of PAM is compatible for foldable robots, the assembly of such actuators remains a complex task.

Milli-scale membrane fluidic actuators, micro-balloon actuators for example [18, 21], are fabricated using advanced techniques including etching, lithography. They are also used in the MEMS field [5]. However, their analytical models cannot be generalized to larger scales, because of their elastic deformations upon inflation are too much [12], and their performances are also limited [26, 27].

1.2.2 Feedback Control

There are also challenges in controlling fluidic actuators. Feedback controls are desirable for foldable robots not only in actuation, but also in the fold-up assembling process. First, during self-folding, the quality of each fold affects the finished geometry and even the performance of the robot. To achieve accurate folds, previous works have been focus on using open-loop control with mechanical stops [9] and redesigning hinge geometry [8]. The later method still results an error of at least 5° [8]. In the sequential self-folding process in [8], the inaccurate folding angles propagates in each step, resulting only 30% of chance

that the robot can successfully fold up. A close loop feedback control is highly desirable as it will not only improve folding quality but also enable the robot to do more complex and controllable tasks.

1.3 Introduce Pouch Motors

This thesis summarizes the works [26–28,34,35]on the developments of pouch motors. Inspired by PAM mechanisms, pouch motors are actuated by compressed air. Since the structure is completely flat, pouch motors are fully compatible with origami inspired robots: they are designed with a computer-aided method, "printed" with various 2D fabrication techniques, and ready to be embedded into a foldable robotic composite laminate. In contrast with other folding methods, pouch motors' actuations are controllable (with a printed sensor), providing a new solution for self-folding, unfolding and continuous actuation. As it is fully customizable, it is now used in robotics and also in Human Computer Interaction (HCI) applications.

1.4 Organization

The paper is divided into two halves: in the first half, from Chapter 2 to 4, I present the fundamental work of pouch motors, including mechanisms, properties, and the full process of making it with an integrable printed sensor layer from concept to fabrication; in the second half, Chapter 5 - 7 are structured to present different variations of pouch motors designs and their applications. Because pouch motors are customized for different applications in the second half of the paper, the analytical model and testing methods introduced in the first half are repeated to allow their performance to be better understood.

In Chapter 2, I categorize pouch motors into two modes of actuations, constructing their theoretical models, and providing testing methods to access their properties. In Chapter 3, I introduce the customizable design and fabrication workflow of pouch motors and the integrable sensor layer, and I evaluate the quality of making. In Chapter 4, I evaluate the use of printed sensor to control pouch motor with angle feedback.In Chapter 5, a specific

angular mode actuation is further studied and used for pneumatic self-folding. In Chapter 6, I extend pouch motor applications into HCI domain by introducing sticker and tape actuators with user studies. In Chapter 7, I review some other pouch motor enabled robotic applications including a legged robot, a robot hand and the Robot Garden Project. Finally in Chapter 8, I conclude the research on pouch motors and discuss the future work with my vision on origami inspired foldable robots.

Chapter 2

Pouch Motor and Mechanisms

The name "Pouch Motor" describes a family of pneumatic actuators made out of two plastic sheets. The flexibility of "thermal drawing" fabrication process contributes to the versatility of pouch motor family. A pouch motor actuating unit can be a single pouch or several pouches connected together. Their actuating mode can be categorized as either "linear" or "angular", but both modes are realized through the change in geometry of the pouch upon inflation and deflation. Note that the word "linear" only refers to the linear motion of driven structure in actuation, and the word "angular" only refers to the rotational motion.

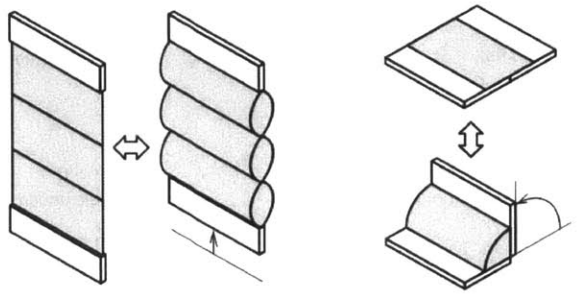

Figure 2-1: Classical pouch motor configuration for two the modes of actuation [27]

2.1 Pouch Motor Family

Figure 2-1 shows an example of each mode of actuation. The pouch motor configuration in these examples are called "classical configurations." The analysis of other pouch motor

configurations can be derived from the classical ones.

2.1.1 Configurations in Linear Mode

In classical pouch motor configuration for linear mode actuation, a multi-unit (or a single-unit) pouch motor connects edges of two structural plates. The total length shrinks upon inflation, which translates into linear motion.

By stacking single pouches on top of another, a "stacked" linear mode pouch motor can be constructed. In this case, the change in height upon inflation is used to actuate motions. The fabrication of this particular pouch motor involves masking using the fiberglass film to prevent heat penetrating through to pre-fabricated films.

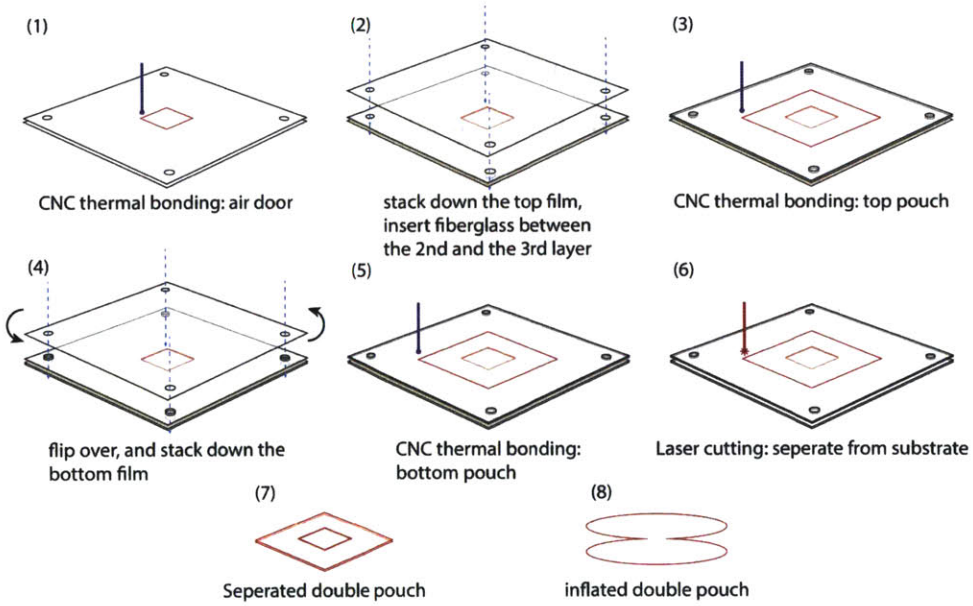

Figure 2-2: stacked double pouch also provides a linear mode actuation (1)-(6): Fabrication, (7)-(8): stacked double pouch [30]

2.1.2 Configurations in Angular Mode

In classical pouch motor configuration for angular mode actuation, a single-unit pouch motor is used.

It is also a common practice to achieve rotational actuation, or "folding", with a multi-unit pouch motor. The two ends of a such pouch motor are attached to two plates of a

hinge. This configuration will be further discussed in Chapter 5.

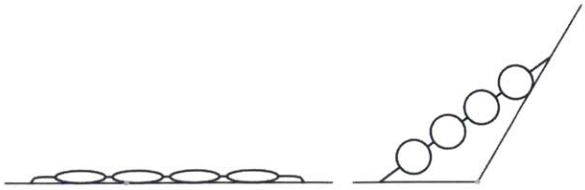

Figure 2-3: Two ends of a multi-unit linear pouch is attached to a hinge. It folds the hinge at inflation

Other configurations in angular mode are also invented. There are three other novel pouches used in the robot garden projetct [30]. One has a spiral design. When this pouch is inflated, it slightly "rotates", as seen in figure 2-4 (middle). Pouch units in figure 2-4 (right) are adhered at one edge. When inflated, the change in height adds up and opens the flower. The pouch motor in figure 2-4 (left) is a slightly different from others: the rotation is caused not so much due to the dimension change, but due to the change in stiffness. When not inflated, the flower is folded to close, but once it is inflated, the pouch becomes stiffer enough to react against the spring force of the paper fold.

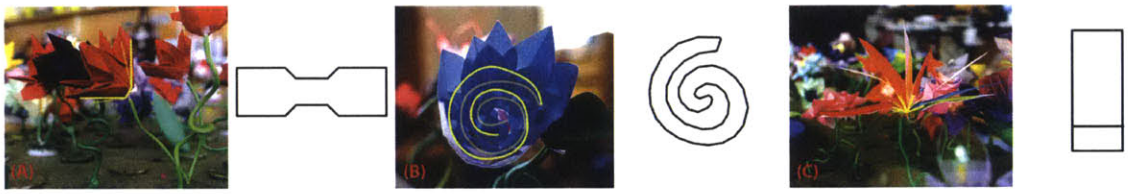

Figure 2-4: Other angular mode pouch motors seen in Robot Garden project [30]

2.2 Theoretical Models

In [26, 27], the classical configurations are discussed in details. They provide important details to help one to understand how a pouch motors work:

As illustrated in figure 2-5, at inflation of a single pouch, the width and length contract but the height expands. If multiple pouches are connected in a certain fashion, the change of one dimension can be exacerbated, therefore generally enhancing the performance. The pouch motors can be attached to the driven mechanical structure in several ways, which decides the mode of actuation to be either "linear" or "angular".

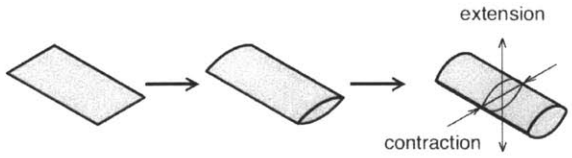

Figure 2-5: Geometry change upon inflation

2.2.1 Analysis of Singe Pouch Geometry Change

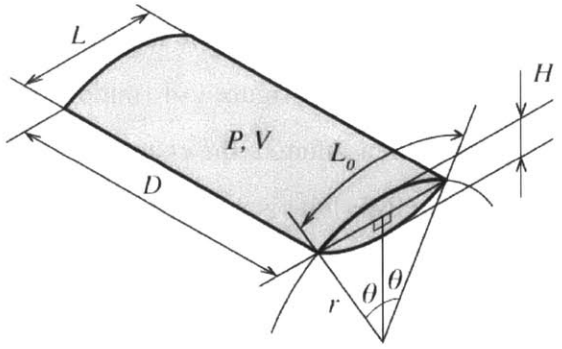

Figure 2-6: Dimensions used on a free pouch

We assume pouch material is not stretchable and has no stiffness against bending. Therefore hoop pressure does not translate into elastic energy. Then with air going into a flat pouch, the pouch inflates, turning top and bottom surfaces to curve and gradually forming a cylindrical shape. During this process, angles of curvature of surfaces θ and L decrease. We assume D does not change.

We use dW_{out} and dW_{in} to represent the output and input work from actuation. Because of the balance of the virtual work,

$$dW_{out} = dW_{in} \tag{2.1}$$

Assume at the end of inflation, the inflated pouch turns into a perfect cylindrical shape. Use L_0 for the initial length of pouch at flat, r for the radius and θ for the central angle of curvature of the top and/or bottom surface, and A for the cross-sectional area of the pouch. We obtain:

$$L_0 = 2r\theta \tag{2.2}$$

$$rsin\theta = L/2 \tag{2.3}$$

$$A = 2r^2\theta - Lrcos\theta \tag{2.4}$$

Therefore we can calculate the length L and volume V of the pouch at any arbitrary angle θ. Note that both L_0 and D are constants:

$$L(\theta) = L_0\frac{sin\theta}{\theta} \tag{2.5}$$

$$V(\theta) = AD = \frac{L_0^2 D}{2}\left(\frac{\theta - cos\theta sin\theta}{\theta^2}\right) \tag{2.6}$$

2.2.2 Analysis of a Single Unit Linear Mode Pouch Motor

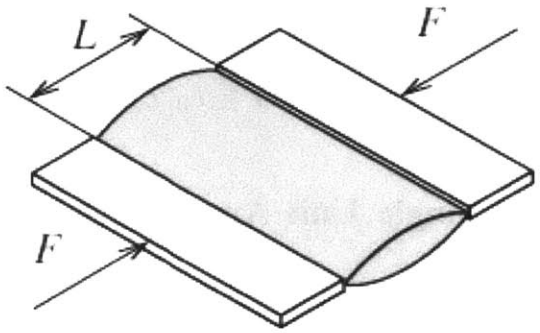

Figure 2-7: A single unit linear mode pouch motor

A linear mode pouch motor produces pneumatic tension force F. Using virtual work from equation 2.1 and equilibrium of energy, we obtain:

$$-FdL = PdV \tag{2.7}$$

where P is the pressure inside the pouch. Therefore,

$$F(\theta) = -P\frac{dV}{dL} = -P\frac{\frac{dV}{d\theta}}{\frac{dL}{d\theta}} \tag{2.8}$$

$$F(\theta) = L_0 DP\frac{cos\theta}{\theta} \tag{2.9}$$

We now define L_e as

$$L_e = \frac{L_0 - L}{L_0} = 1 - \frac{sin\theta}{\theta} \tag{2.10}$$

L_e only represents an ideal case, because in an actual case, the pouch material stretches upon inflation. We now use a corrected term L'_e to better describe contraction ratio, that

$$L'_e(\theta) = L_e\left(1 + \frac{\pi d}{\pi - 2}\right) \tag{2.11}$$

In this case, d is a correcting constant, and C_e is a coefficient of the strain, that:

$$d = C_e P \tag{2.12}$$

It's worth noting that L'_e and L_e are consistent when $\theta = \pi/2$ and $F(\theta) = 0$, at which produces the maximum contraction value, which is $L_e(\pi/2) = L'_e(\pi/2) = \frac{\pi-2}{\pi} \approxeq 0.363$. In addition, the maximum force produced is at $L = L_0$, $L'_e = 0$.

2.2.3 Analysis of a Single Unit Angular Mode Pouch Motor (ideal model)

A single unit angular mode pouch motor can be made in two ways. The first one is simply two tabs completely separated and adhered to the pouch. We call this the "ideal model".

A angular mode pouch motor produces pneumatic moment M. Using virtual work from equation 2.1 and equilibrium of energy, we obtain:

$$Md\phi = PdV \tag{2.13}$$

where ϕ is the angle produced. It can be found with θ that

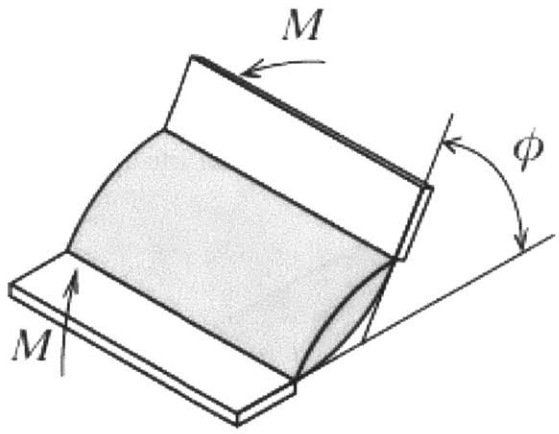

Figure 2-8: A single unit angular mode pouch motor in ideal model

$$\phi(\theta) = 2\theta \tag{2.14}$$

Therefore we can find moment produced as a function of θ that

$$M(\theta) = P\frac{dV}{d\phi} = P\frac{\frac{dV}{d\theta}}{\frac{d\phi}{d\theta}} \tag{2.15}$$

$$M(\theta) = L_0^2 DP\frac{cos\theta\,(sin\theta - \theta cos\theta)}{2\theta^3} \tag{2.16}$$

In angular mode, the range of motion is π. The maximum moment is produced at $\phi = 0$.

In ideal model, attached mechanical structures have to be assumed weightless, because if there is a weight, they will be likely to dig into the pouch when loaded. Realizing this issue, the hinged model is created: instead of using the pouch to attach two separated tabs, we made the compliant hinge with the pouch attached.

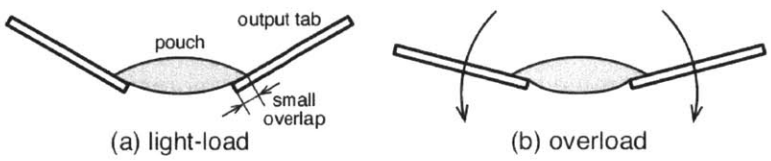

Figure 2-9: An ideal model single unit angular pouch motor with load

2.2.4 Analysis of a Single Unit Angular Mode Pouch Motor (hinged model)

The "hinged model" set up is usually better in real-life applications.

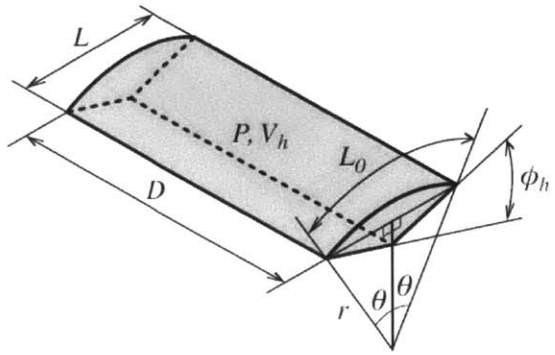

Figure 2-10: Dimensions used on a hinged pouch

The volume of a hinged model can be calculated similar to equation 2.6 for the ideal model:

$$V_h(\theta) = A_h D = L_0^2 D \left(\frac{\theta - cos\theta sin\theta + sin\theta\sqrt{\theta^2 - sin^2\theta}}{4\theta^2} \right) \tag{2.17}$$

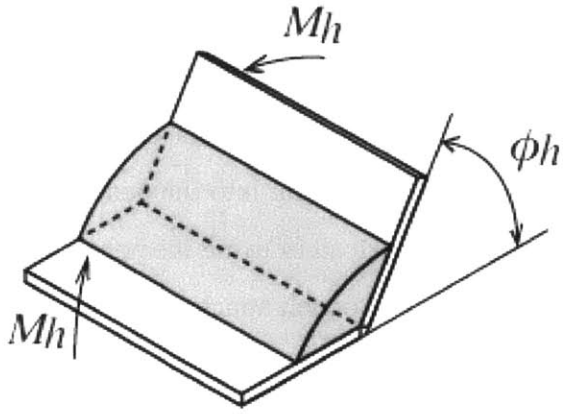

Figure 2-11: A single unit angular mode pouch motor in hinged model

The angle produced ϕ_h from a hinged model in terms of θ can be expressed:

$$\phi_h(\theta) = arccos\left(\frac{2sin^2\theta}{\theta^2} - 1\right) = 2arccos\left(\frac{sin\theta}{\theta}\right) \tag{2.18}$$

Its moment M_h can be found by plugging 2.17 and 2.18 into equation 2.15, that:

$$M_h(\theta) = \frac{L_0^2 DP}{8\theta^2}\left(-1+\theta^2+cos2\theta-\sqrt{2}cos\theta\sqrt{-1+2\theta^2+cos2\theta}\right) \tag{2.19}$$

Theoretically, a hinged angular pouch motor can produce a range of motion from 0° to 93.4°. When the hinge is flat the moment is the maximum.

2.3 Performance Assessment Method

We built two testing fixtures to measure the performance of a typical multi-unit pouch motor and a single unit pouch motor [26,27]. This section explains the process of assessment on each mode using classical pouch configuration as the example. We will conduct same study on other configurations in later chapters.

2.3.1 Properties of a Multi-Unit Linear Mode Pouch Motor

A three-unit linear mode pouch motor made with line sealer from a 4mil (0.102mm) PVC film is used for this assessment. At deflated state, each unit is 8.5cm wide(D), 2.5cm long(L_0). It has a coefficient (C_e) of $1.667x10^{-6}Pa^{-1}$.

The assessment is a quasi-static process. Before the assessment, the pouch motor is relaxed (deflated) and barely pulling the force sensor. The assessment starts with air streaming into the pouch. The pressure is maintained once it reaches a desired steady level throughout the experiment. Because of the inflation, the pouch motor contracts and pulls the force sensor. Then the contraction is manually adjusted. The top tap is cranked down until the pulling force measured at the force sensor reaches zero, and then cranked up back to the starting position.

We used equation 2.8 and 2.11 at $0 < \theta \leq \pi/2$ to construct a parametric plot of the mathematical model. It is compared against an experimental plot in figure 2-13.

Hysteresis is observed on the experimental plot, which reflects the plastic nature of the pouch film material. The maximum contraction ratio observed is about 28%, which is

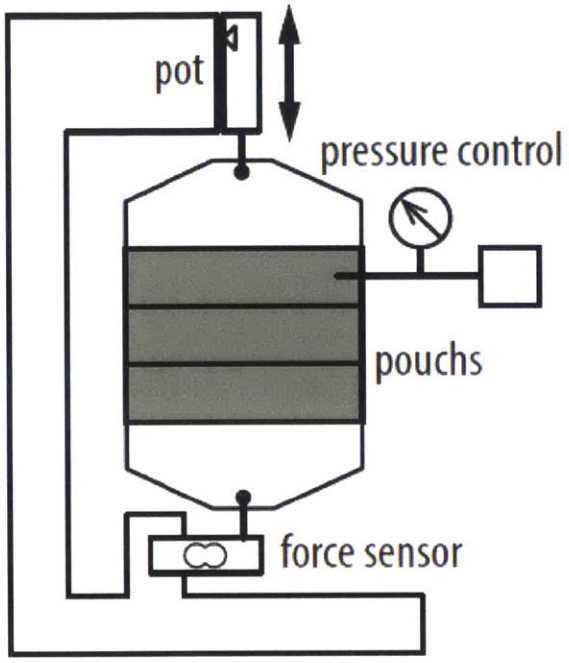

Figure 2-12: Linear actuation testing fixture

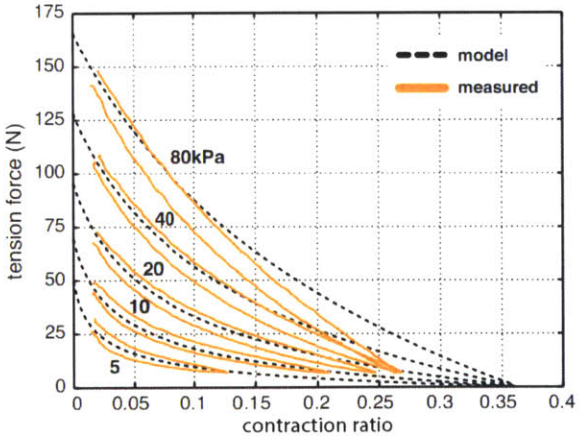

Figure 2-13: Plots of the theoretical model in linear mode and an experimental result

comparable to McKibben artificial muscle [4].

The experimental data agrees with theoretical plot more when pressure is lower. In our mathematical model, we assumed material to be non-stretchable. The contraction ratio been less than predicted. It is probably due to the fact that the sheet PVC material is still stretchable at some extend especially at a higher pressure.

2.3.2 Properties of a Single Unit Angular Mode Pouch Motor

A single unit angular mode pouch motor made with the same method from the same material is used for this assessment. At deflated state, the pouch is 10cm wide(D) and 2.5cm wide (D).

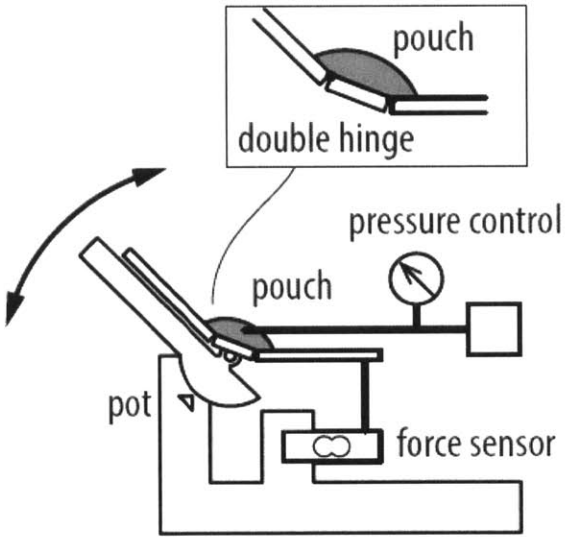

Figure 2-14: Angular actuation testing fixture

The angular mode assessment is also quasi-static and performed just like the linear one. Instead of controlling the contraction ratio, in this case we controlled the turning of the hinge (folding angle), from flat to an angle at which $M = 0$, and then back to flat.

Because the pouch is adhered to the flat surface of the tabs, to keep the inflated pouch shape as cylindrical as possible (to keep it close to the mathematical model), we used a double hinge design in this experiment: two hinged models are used on the same pouch.

Equation 2.18 and 2.19 are used at $0 < \theta \leq \pi/2$ to construct a parametric plot of the mathematical model. It is compared against an experimental plot in figure 2-15.

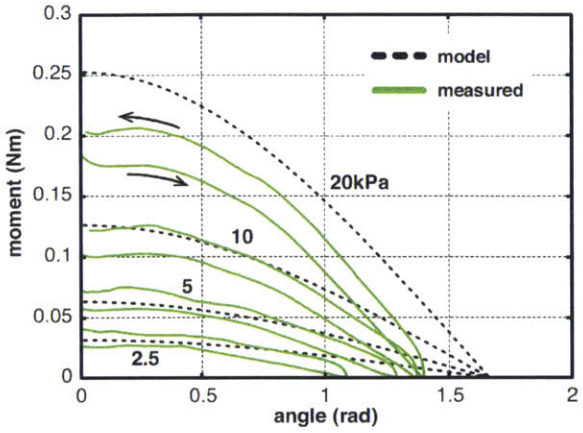

Figure 2-15: Plots of the theoretical model in angular mode and an experimental result

Like the linear mode test, again experimental plot and mathematical model have close matches at lower pressures. This may due to the same reason that in the mathematical model the material is assumed non-stretchable. The stretching may have taken place during experiment and bring down moment at higher pressure.

Chapter 3

Design and Fabrication

3.1 Overview of Pouch Motor Driven Origami Inspired Robots

Like other self-folding robots [8, 9, 14, 15, 20], pouch motor driven origami inspired robots are folded up from planar laminate materials. Depends on the application, the construction of the laminate material can vary. Here I list a complete set of layers of materials that can be included in a such laminate.

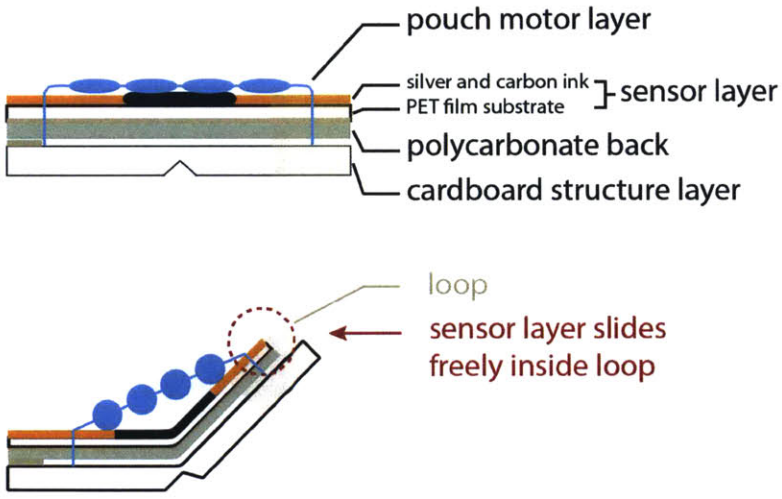

Figure 3-1: A complete set of layers for pouch motor driven foldable robots. Top: flat state showing names of each layers; Bottom: actuated state. Pouch motors are inflated to fold the hinge to an angle

Each layer is made with a separate planar fabrication process and then they are stacked and adhered together. Therefore before folding up a robot from the laminate, design and fabrication of each layer needs to be done.

This chapter will talk about how pouch motors are designed and its three possible planer fabrication processes (based on our work in [27]). Additionally, the sensor layer design and fabrication, and its quality assessment are discussed. It will also include how other layers are made and finally how robot laminate is put together (based on our work in [35]).

3.2 Pouch motor layer design

Pouch motor layer can be made with three methods: by heat drawing, by de-focused laser drawing or by heat stamping. Heat drawing and de-focused laser drawing are very flexible in customization. Heat drawing is usually favored in prototyping. Whereas heat stamping process is usually faster and can be very useful for large scale manufacturing.

Depends on the type of fabrication, the design process is slightly different. For heat drawing and de-focused laser drawing, pouch motors can either be co-designed with developed algorithms [27] or designed from a Computer Aided Design (CAD) program. The output from the design stage is a dxf file. The fabrication stage takes the design file and either machines out a "stamp" for heat stamping, or converts it into G codes and uses either a heat drawing machine or a laser cutter to "draw" pouches on thermal plastic sheets.

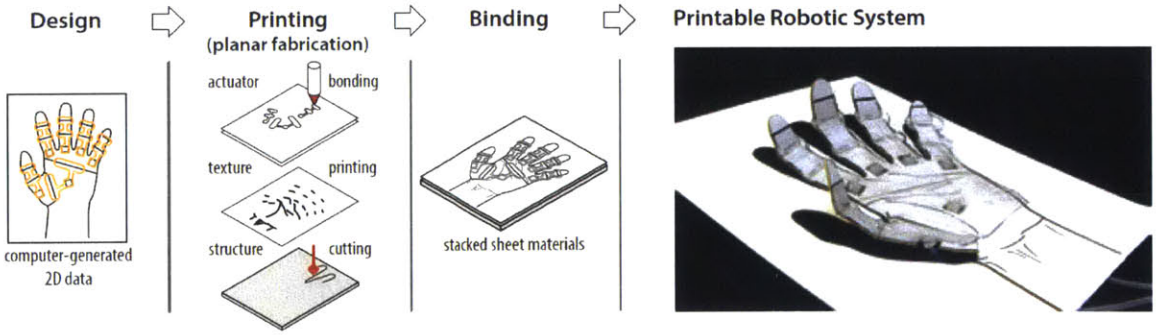

Figure 3-2: Overview of pouch motor drawing fabrication workflow

In most applications, multiple pouch motors are used. They are grouped by the sequence of actuation. Within each group, pouches are connected with printed air channels.

A modified tubbing connector is used to interface a tube to a pouch group. The other end of the tube connects to valves that either supply air or exhaust air. Because a pouch network is application specific, it is necessary to have functionality defined before designing or making pouches.

3.2.1 Design by a CAD program

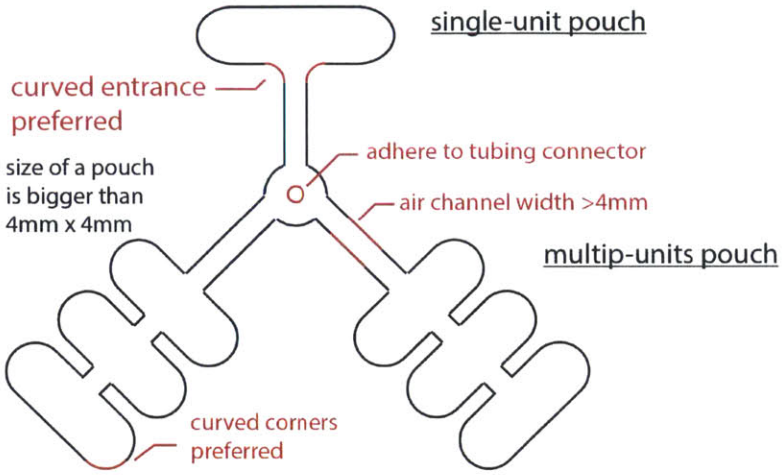

Figure 3-3: A example of a printed pouch motor network containing one single-unit pouch and two multi-units pouch

As mentioned above, the "drawing" processes produce designs of pouches from CAD whereas "stamping" produces the design of the stamp. Regardless the method, over times of making and using pouch motors, an empirical guideline for designing has formed:

- For smooth air streams, the width of an air channel should be bigger than 4mm;
- An air channel should connect to a pouch with curved entrance, with a radius of around 2mm;
- The pouch should have curved corners, ideally with a radius of around 2mm;
- To create noticeable geometry changes, the size of the pouch should be larger than 4mm by 4mm;
- Sharp angles should be avoided in a pouch network if possible;

- Air channels can't be bent or folded during application, as it will jam air;

3.2.2 Co-design with robotic definition

Ryuma et al. developed an algorithm to semi-automate pouch designs based on the mechanical design of the robot [27]. It creates pouch motors with the following steps:

1. The flat mechanical structure is defined with hinge and port positions located. The ports and actuated hinges are grouped.
2. The algorithm generates routes of shortest Euclidean distance.
3. Pouches are placed on the folds with routes evenly placed across the folds
4. Routes are replaced to stay within the boundary of the substrate and evened out the space from the edge to any other routes or pouches.
5. The air channels and tubbing interfaces are produced.

3.3 Pouch motor planar Fabrication

3.3.1 Heat Stamping

A stamping block's 3D design is produced at the end of design work flow. It is made by CNC machining at the beginning before pouch fabrication. The stamp is mounted onto a heat press. A layer of 0.127mm (5mil) PTFE fiberglass and two layers of thermal plastic films are stacked into the machine. The fiberglass serves to prevent the heated stamp to over-melt and stick to thermoplastic films. In a demo, we used 0.102mm (4 mil) vinyl films. After the heat press is turned up to a desired temperature around 245 °C, the heat press can be pressed closed for around 5 seconds. The molten films are then taken out to cool down. The printed pouch motor network is then separated from the films with a pair of scissors.

A variety of factors influencing the quality of pouch motors are found, as shown in table 3.1.

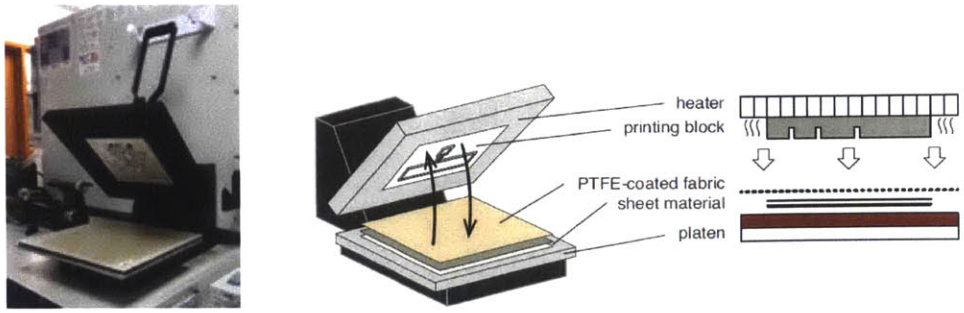

Figure 3-4: Heat Stamping Process

3.3.2 Heat Drawing

The drawing of a pouch network is produced at the end of the design work flow. A CAM software interprets the design into G-codes, which then is loaded into a customized CNC machine and ready for heat drawing. This customized CNC machine has a few special features. First, it holds a soldering iron which is pressed into drawing canvas during the fabrication. A linear spring allows the Z-axis holder to travel into "negative" space, which in reality, linearly increasing the pressing force of the tip of the soldering iron against the canvas. Second, a rubber board is adhered on the canvas to hold the films. This board ensures that the soldering iron has a consistent contact with the films.

At the beginning of a demo fabrication, a layer of 0.127mm (5mil) PTFE fiberglass and two layers of thermal plastic films are stacked on the top of the drawing rubber canvas. The fiberglass in this case serves to minimize the friction between the soldering iron tip and the films. The soldering iron is turned on to 357 °C. Once the machine is turned on to run, the computer takes a line of G-code and controls the movement of the soldering iron to "draw" the pattern of the pouch network onto the films. In our case, we set the speed of drawing to be 375 mm/min and drawing force to be 6.9N. Once the drawing is finished, pouch motors are cut off from the films. The factors influencing the quality of make are recorded in table 3.1.

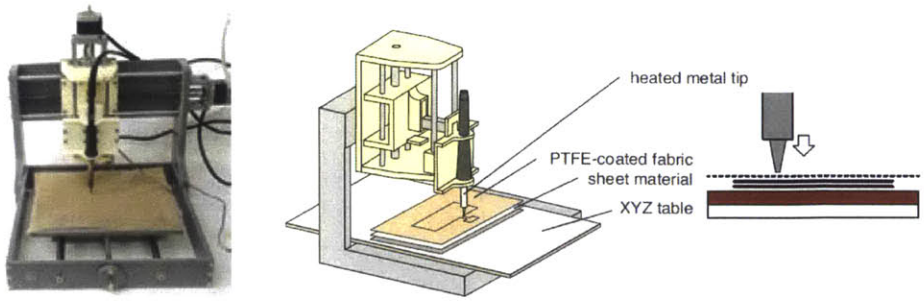

Figure 3-5: Heat Drawing Process

3.3.3 De-focused Laser Drawing

De-focused laser drawing is very similar to heat drawing. It is a contactless "drawing" process - in stead of using soldering iron that touches films, the machine directs de-focused laser to the films.

Two layers of thermal plastic sheets are loaded into a CO_2 laser cutter and held in place with weights on the sides. Since cutting PVC produces toxic chlorine gas, we use 0.102mm (4mil) PTFE films instead. In the laser cutter setting, the mode is set to "vector", the speed is set to 45%, the power is set to 15%, frequency is set to 5000Hz. Before the laser drawing begin, focus is set to be 0.6 below the true focus surface.

It is noted that thin films are usually easily corrugated. When the laser is emitted onto the films, heat does not propagate evenly, causing poor bonding quality. Even the pouch is completely formed, it does not withstand high air pressure. As a result, this methods is barely used in applications.

3.3.4 Stamping vs. Heat Drawing

Heat stamping and heat drawing processes are different in many ways, mainly including cost of making, customization flexibility and fabrication time.

Heat stamping process costs more. Every time before making one pouch design, a stamping block needs to be machined. It also cost more on energy consumption as the heat press need to be heated up before fabrication and is on through out the process.

Heat drawing is very customizable. Heat stamping on the other hand only prints the

design of a mold. Both methods, however, are limited in resolution of the drawing, and the size is dependent on the machine size.

Although it takes time to machine a stamping block, once it is made, the time it takes to replicate one pouch motor network design is very fast. Heat drawing takes much longer time, especially when the design of a pouch network is complicated, or there are multiple separated pouch groups.

Considering cost, time and customizability, generally heat drawing is ideal for prototyping and heat stamping is ideal for mass manufacturing.

We also compared the factors that influence the quality of make with these two methods in the table below:

Table 3.1: Fabrication Parameters

	Heat Stamping	Heat Drawing
Line Width	Stamp pattern width	tip diameter, drawing force, board rigidity
Temperature	Stamp temperature	tip temperature
Process time	Stamping time	Drawing speed
Sealing force	Stamping pressure	Drawing force

3.4 Sensor layer Design

The sensor layer is a PET film (Mitsubishi Imaging item number NB3GUA4X100) on which multiple angle sensors and connecting circuit are printed by a piezoelectric inkjet printer [35]. The sensors are printed with carbon nano particle ink. When they are folded, the distance between deposited carbon nano particle changes, resulting a change in its total resistance. By measuring the resistance change, one can calculate the folding angle. The circuitry part that connects sensors are printed with silver ink. The PET substrate can be replaced with a glossy photo paper. However, PET has higher stiffness than glossy paper. The extra stiffness helps the hinge to unfold from a folded angle and is usually desirable in many applications.

The sensor included circuit can be designed in any vector-based drawing or CAD programs. To print carbon and silver ink from the same printer, simply load carbon ink in the

black cartridge and silver ink in all color cartridges. When designing, black color is used to draw sensors and a saturated color cartridge color (cyan, purple or yellow) is used to draw the circuitry. Based on previous works on inkjet circuit printing [17], the printer setting for Brother DCP-J152W is optimized to print both circuit and sensors in table 3.2.

Table 3.2: Printer Settings

	Print Silver ink	Print Carbon ink
Media Type	Other photo paper	Plain paper
Print Quality	Best	Best
Color Mode	Vivid	N/A
Color/ GreyScale	Color	Grey scale
Color Enhancement	checked	checked
Color Density	+2	N/A
Improved Pattern Printing	Checked	Checked

3.5 Sensor layer fabrication

3.5.1 Fabrication by printing

After a few times printing, broken lines are commonly observed on printed sensor. This is because even with the modified printer setting, printer is not capable to automatically do enough cleaning to remove excessive large silver and carbon particles. It is advised to clean the printhead regularly with the built-in cleaning function.

Because the setting for circuit and sensors are different, they need to be printed separately. The circuit is printed first with proper settings shown in the first column in table 3.2. Then the PET film with printed circuit is carefully feedback into the printer to print sensors with settings shown in column 2. The sensors should be printed repeatedly for at least three times to prevent those broken lines.

3.5.2 Fabrication Quality

Theoretically we can design the sensor resistance directly be using different widths and lengths. If the sensor is printed just once, it has a sheet resistance of $R_s = 5k\Omega/\square$. We also know that

$$R = R_s \frac{L}{W} \tag{3.1}$$

Realistically this does not yield a good estimate of the actual resistance. This is largely because the printer we use does not produce good enough quality due to random clogging. The printed sensor (with only one layer of carbon ink) is taken to a closer examination with an optical microscope.

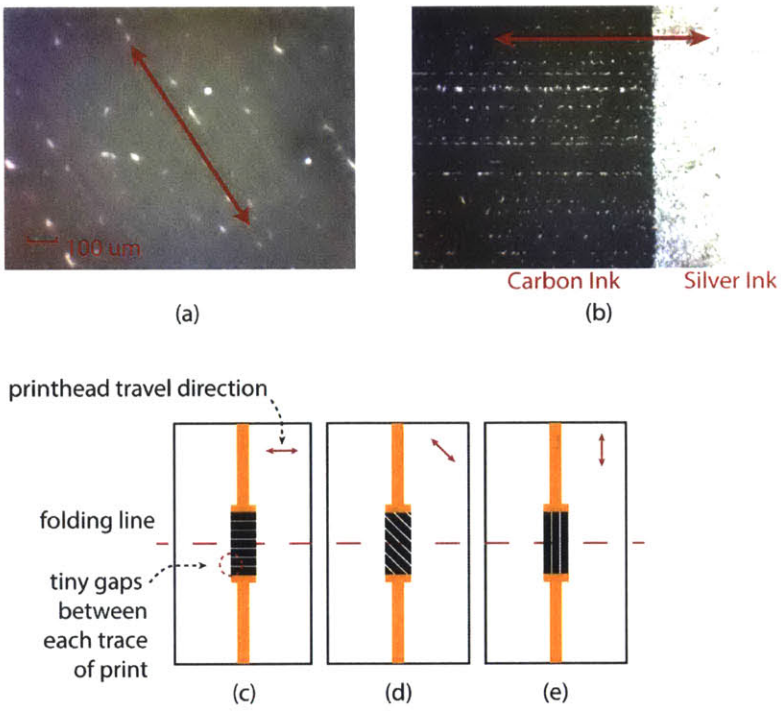

Figure 3-6: Print head travel direction and gaps between each trace are observed. (a) a closer look at the sensor part, white dots are unprinted gaps (b) comparing print quality of carbon ink and silver ink (c), (d) and (e) illustrate the samples for quality testing. Their print head travel direction and gaps orientated differently with respect to folding line

Carbon particles appear to be bigger than silver particles. Certain orientation of the gaps resulted from clogging with respect to folding line can make sensor more resistive, making printed sensor resistance inconsistent. To further study how this affects the resistance, three

groups of ten samples are prepared. Sensors in the first group are placed 0° (Fig. 3-6c); sensors in the second group are placed 45° (Fig. 3-6d) and sensors in the third group are oriented 90° (Fig. 3-6e). Resistance at unfolded (flat) and folded (90°) states are recorded. The findings are as below:

- At the unfolded state, samples within the same group have different resistances. The largest standard deviation of 9.8° is seen in group in Fig. 3-6c. This is likely because as ink clogs printhead, less ink is deposited per unit area over time to conduct electricity.

- At the unfolded state, the average resistances of each group are calculated and found to be different. In Fig. 3-6, the connectivity in the vertical direction is more important than other directions. As the printhead travel directions in each case is different, it breaks connectivity in different orientations.

- When comparing the unfolded to the folded state, the average change in normalized resistances in all groups are found to be very close. The standard deviation is only 2.2%.

As printed sensors do not have coherent resistive property, the resistance always need to be measured after fabrication to optimize control applications. The change in resistance from flat to 90° fold angle are consistent, indicating them good candidates to implement in feedback control.

3.6 Fabrication of other layers

Polycarbonate back layer (as shown in Fig. 3-1) is cut out with scissors. Springback force is usually helpful for the folded joint to unfold. Although sensor layer PET substrate already a small springback force, it is enhanced with the additional polycarbonate back. The polycarbonate back also makes the sensor to fold at larger radius of curvature, making the distance between carbon particles on the print to stretch evenly and produce better readings. After cutting, it is adhered to the sensor layer with double sided tape.

Cardboard is usually used as the structural layer of the robot. Its profile is drawn based on the desired 3D folded geometry. There are several algorithms developed to design folded robots with some prime units, which directly produces unfolded patterns, such as in [23]. Users can also simply draw the unfolded pattern with a vector drawing program or a CAD program. A layered composite cardboard is placed inside a laser cutter. The profiles are cut and the hinges are grooved at a lower laser power.

If the sensor layer is used, only one end of the sensor layer (of polycarbonate back) is taped onto one side of the cardboard hinge. A strapped loop made with some scotch tape is made on the other end, allowing the sensor layer to slide freely when bent. The pouch motor layer stays at the top, which can pull up the hinge to fold at inflation. When pressure is relieved from the pouch, the polycarbonate and the PET film pull down the hinge to unfold.

Chapter 4

Feedback Control with Printed Sensor

The design and fabrication of a printed sensor layer is described in the last chapter. The performance will be studied in this chapter with some application examples validating its use in foldable robotics domain (based on our work in [35]).

4.1 Performance Study

4.1.1 Electrical Properties

An ideal Sensor has consistent electrical behaviors over a wide range of applied voltages. In this test a 4.5mm by 20mm printed sensor at the unfolded state (laying flat) is applied with an increasing voltage at 1 volt intervals from 1V to 16V. The corresponding currents flowing through are measured. The result is plotted in 4-1 shows that the sensor has a linear ohmic Voltage-Current behavior in this range.

4.1.2 Angle reading tests setup

To access how well the sensor can read a folding angle, a testing hinge fixture is constructed with a dial type potentiometer and a servo motor. As the servo motor turns the tab, the connected potentiometer reads the true folding angle, while at the same time, the printed sensor also takes a reading. The testing sample is mounted on the top of the fixture. As the right tab folds up, the sample hinge also folds to the same angle. This setup is shown in

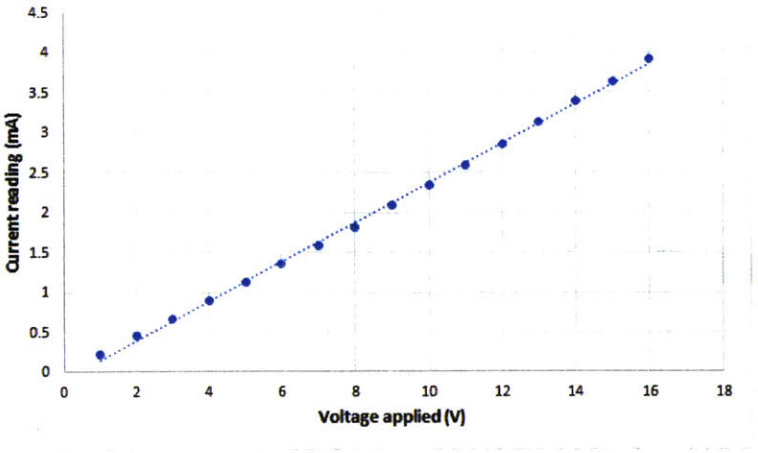

Figure 4-1: Electrical property of the printed sensor

4-2.

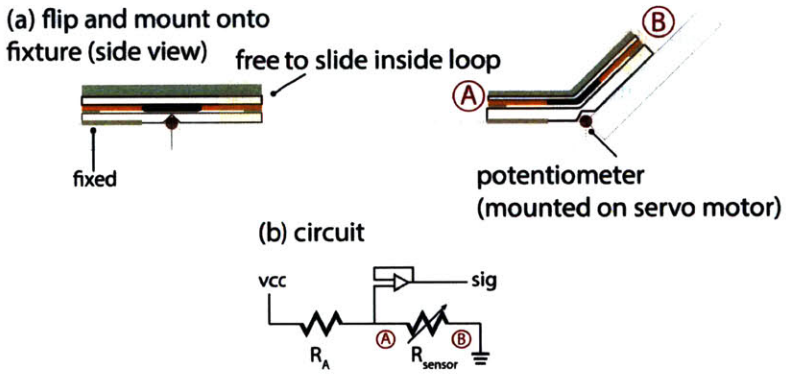

Figure 4-2: Testing hardware setup

To filter out noise, multiple printed sensor readings are taken at the same folding angle and averaged. From early experiments, a delay is found between the time of fold and actual change in sensor reading. This may be because the PET substrate is a viscoelastic material. To compensate this effect, the program is coded to wait for a few seconds (t_{wait}) before a recording a new reading.

4.1.3 Varying folding speed

In the first experiment, trials are run with different servo folding angular velocities (by changing t_{wait}) to study how the folding rate affect the readings. In Fig. 4-3, 5.9°/s, 3.2°/s, and 0.4°/s folding velocities are used to fold the hinge from flat (0°) to 60°. All three trials

produce a same linear relationship between the commanded angle and the measured actual angle with a standard deviation of 2°, 1°, and 2°, degrees respectively.

It is therefore found that the speed of folding does not have much effect on sensor behavior. At higher folding speeds, small raise in readings are found at the beginning of the plot (from 0° to 15°). This may be attributed to hinge accelerating to flat state from folded state of the last trial.

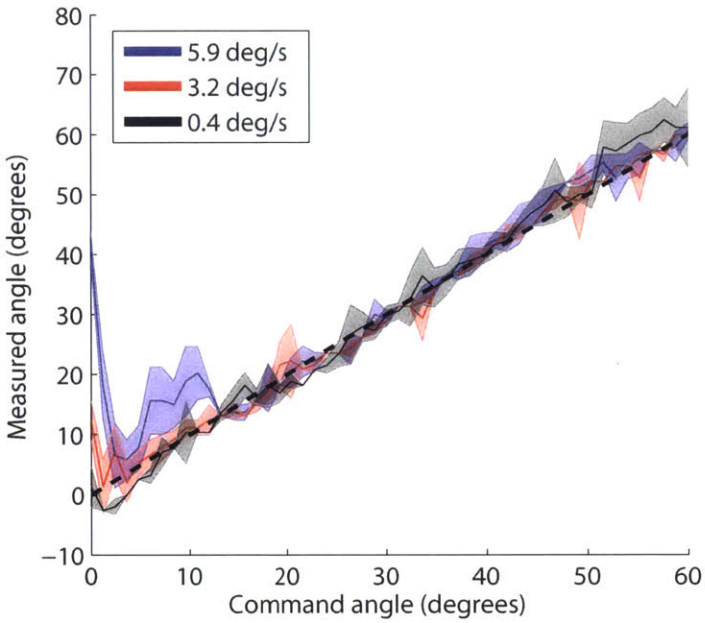

Figure 4-3: Measured angle as a function of command angle at three different speeds: 5.9°/s, 3.2°/s, and 0.4°/s. The shaded region indicates standard deviation, N=4. The dashed line indicates the true angle.

4.1.4 Repeatability

It is also an important measure that the sensor needs to produce expected results repeatably. In the second test, the servo repeatedly folds the hinge to 30° from flat (0°) quickly for 30 times are the results are recorded as shown in 4-4. Every time when the servo folds, the 30° angle is achieved within 0.5s. The plot shows that the reading drops overtime. This may be a result of viscoelastic material's stress relaxation. The standard deviation after one second time mark is 2°. This result is higher than the sensor first folded, probably due to the PET

substrate settles in some ways.

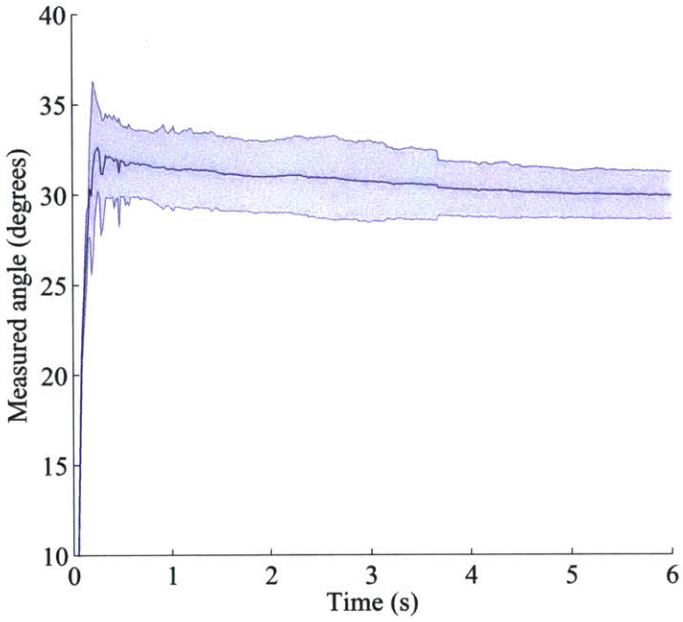

Figure 4-4: Measured angle of a hinge upon near instantaneous (<0.5 s) folding to 30°. The shaded region indicates the standard deviation, N=30.

4.1.5 Sensor width effects

Sensor quality is found to be dependent of ink layer thickness, as explored in last chapter. It is also found to be dependent on the width in angle reading experiments. Four samples of the same length (12mm) but different width (2mm, 4mm, 8mm and 16mm) are prepared to conducted the angle reading test with the same folding speed from flat (0°) to 60° fold for thirty times, and their average error bar as compare to the commanded angle are recorded as shown in Fig. 4-5. It is found that as width increases above 8mm, the error in measuring angle becomes smaller. This may be because as the width increases, random gaps from fabrication are compromised more as the current can go through more paths along the sensor.

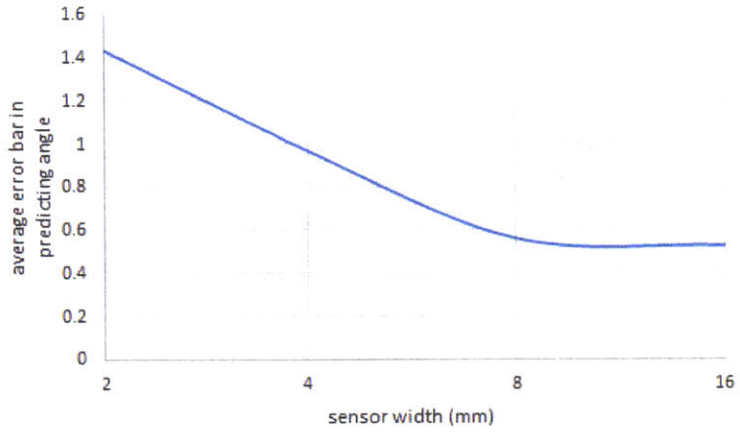

Figure 4-5: Effect on angle reading accuracy from sensor width

4.1.6 Feedback control validation

The feedback control is validated in a simple bang-bang control experiment. Using the same setup in Fig. 3-1 without a servo, true folding angle is measured with the connected dial potentiometer. The pouch motor on the hinge is connected to a pressure source and a pressure relieve valve. The printed sensor on the hinge is first calibrated. During the experiment, microprocessor command the hinge to turn to an angle with 5° steps from 0° to 25°. If the printed sensor detects that the hinge is one degree below the desired angle, the exhaust valve shuts but supply valve opens to inflate the pouch. If the sensor detects that the hinge is one degree above the desired angle, the supply valve shuts but the exhaust valve opens to leak out some air. At the same time through out the experiment, the potentiometer records the true folding angle. Commanded angles, potentiometer readings, and sensor readings are all plotted in the same time scale, as shown in 4-6. The sensor produces accurate readings, making the hinge to stay within a 2° range from the commanded angle. The readings at lower angles (especially at 0°) are less accurate. This may be because the sensor film has some local sag and does not return to a perfect flat surface.

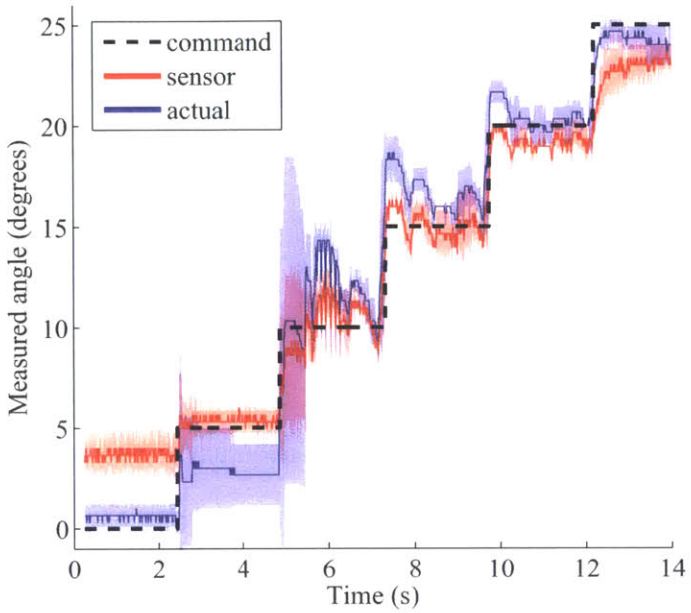

Figure 4-6: Command signal (dashed), printed sensor reading (red) and actual angle (blue) of the hinge. The actual angle is measured by a potentiometer attached to the hinge. Shaded region indicates standard deviation, N=3

4.2 Applications

4.2.1 Tracking the fold of a cube

To demonstrate the versatility of how the printed sensor can be used to track folding, a cube cardboard structure embedding the sensor layer is made. The foldings of the cube are tracked and animated on a computer, as shown in Fig. 4-7. The cube is first calibrated by recording a reading at 0° and a reading at 90° and assuming linear angle to reading relationship in between. During application, every time before microprocessor output an angle reading, it first takes a 2.5s delay to allow the reading to settle and reads angle forty times and output the average of all readings as the final reading. The demonstration can be seen in the supplemental video in [35].

Because of this reading procedure, it takes about 3s in total before the a new reading is produced and animated on the computer. It helped the folding angles between 0° to 90° to be tracked within an error bar of about 5°.

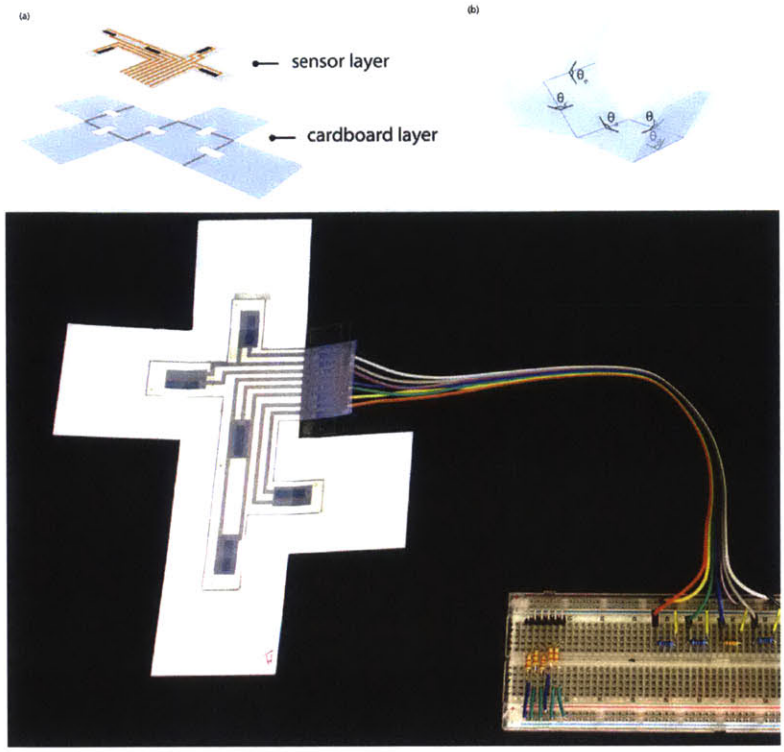

Figure 4-7: (a) sensor layer embedded in an unfolded cube (b) shows the angles it tracks (c) final cube model

4.2.2 Controlling a Gripper

A five-finger gripper actuated with pouch motors are made to demonstrate feedback control. Sensors are printed only below the five knuckle joints of the grippers. Microprocessor controls the folding of the knuckle joints with the printed sensor, just like the bang-bang control example setup before. Because all pouches are connected together sharing the same pressure, it is assumed that the folding angles of all five knuckle joints are the same. This way, five data are taken once and the reading time is reduced by 80%.

The sensors are calibrated as in the cube folding case. The feedback control is done with a 4° range as compared to 1° in validation experiment. During the application, because the pouch motors are not adhered exactly the same positions relative to the knuckle joint positions, they don't fold to the same angle. This contributes significantly to errors in control compare to the validation experiment.

To illustrate feedback control, when the knuckle joints are folded at 60°, the gripper is forced to open (turning fingers to smaller folding angles). The sensor immediately detects

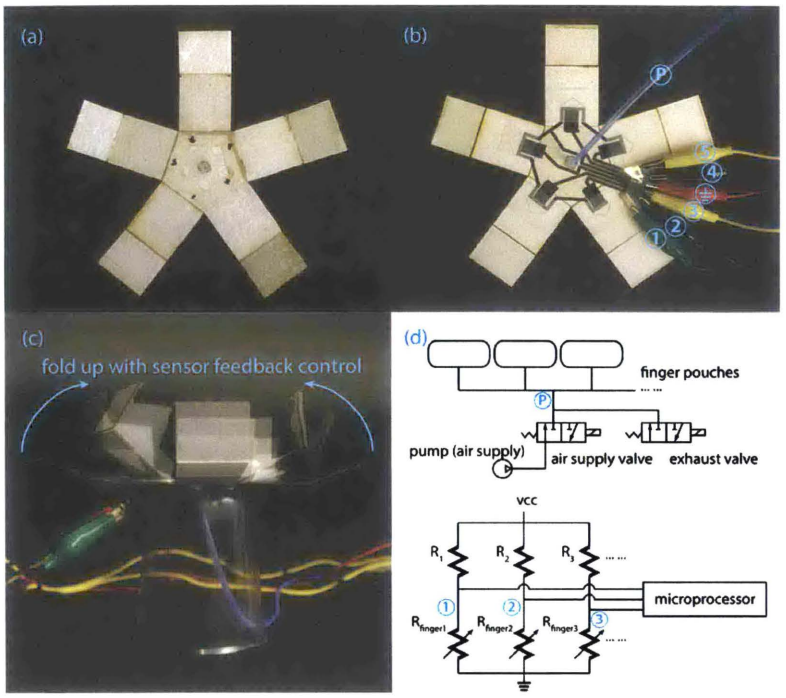

Figure 4-8: (a) gripper top view: pouch motor layer; (b) gripper bottom view: sensor layer. The connection are marked corresponding to the control circuits in (d); (c) gripper folding in action; (d) shows the pneumatic and circuits control

the angle change and allowing more pressurized air to enter to compensate. Again, this can be seen in the supplemental video for [35].

4.3 Discussion

In this chapter, the sensor layer properties are further explored with a variety of tests. It is found that it produces readings approximately close to linearly to the folding angles. It responds to a fold in about 0.5 seconds and produces a reading within a range of 2° to the true folding angle. The sensor is validated to be applied in feedback control settings, and demonstrated in applications.

The printed sensor still needs to be further studied to be reliably coupled with pouch motor driven foldable robots. First, the true relationship between the angle and sensor readings need to be understood. The linear model used are based on observations. Second, the resistance of the sensors drift over time in the scale of days. Third, variance in readings,

although workable in some robotic applications, may not be acceptable in others. These two shortfalls may be attributed to the poor print quality of the printer used and may improve with a more reliable printers.

Chapter 5

Robot Pneumatic Self-Folding and Actuation

The concept of robot self-folding allow robots to be transported easily and can assembled autonomously. They have been realized through SMA and SMP mechanisms. However, shape memory material foldings are irreversible and it is hard to control folding angles.

In contrast, pouch motor actuations are reversible and controllable with pressure when the loading force is known. It provides an alternative solution to fold robots with advantages.

In this chapter, instead of using printed sensor to control folds, pressure based open loop controls are explored. The angular mode pouch motor used in this chapter has the same configuration like the one used in the previous chapter (Fig. 2-3, Fig. 5-2).

This chapter is based on our work in [34].

5.1 Analytical Model to Pouch Actuated Folding

5.1.1 Theoretical Model

A basic hinge unit is illustrated in Fig. 5-2. As the sensor layer is not utilized, to keep the springback mechanism, we added a flexure film (polyester either 2 mil or 10 mil) which makes the fold always tight.

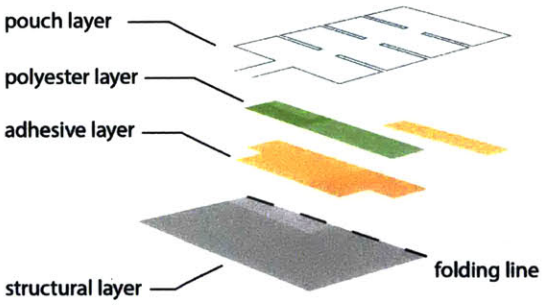

Figure 5-1: Basic construction of a pouch actuated hinge

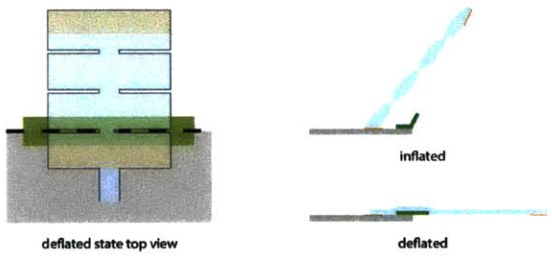

Figure 5-2: Actuating a pouch on a fold

In chapter 2, we developed an analytical model for a multi-unit linear mode pouch motor. In that model, pouch pressure, contraction ratio and force are dependent on each other. In this modified case, we assume external torque compare to the reflection torque from the flexure are negligible, and that the pneumatic energy are balanced out from the flexure bending. This leaving the pouch folding angle controllable from just the air pressure.

We developed a more precise model based on the multi-unit linear mode model as in chpater 2. We first keep the same assumption that as pouch infinites, it forms a perfect cylindrical shape. The total length of the pouch between two attachment points at folding is L_{min}, and at complete deflation is L_0. When pouches fully inflated, the fold angle is ϕ and the angle inside the hinge is ψ. The two distances between attachment points to the hinge are L_1 and L_2 respectively, and actauted length is L_3. The actuator displaces x and the total length of inelastic region is L_e. Since we know that this perfect deformation is not achievable to 100%, and therefore use a shape factor ε to take an account of the oval-like geometry.

We use the same variable name to the single pouch. Both are shown as in Fig. 5-3.

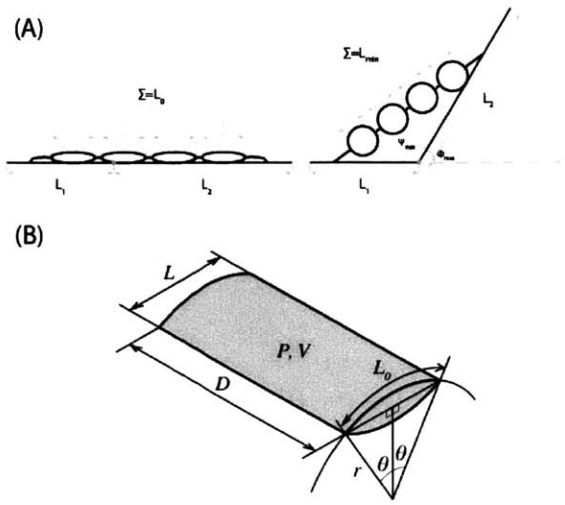

Figure 5-3: (A) parameters used on a joint (B) parameters used on a single pouch [26]

$$x_{max} = L_0 - L_{min} = \varepsilon \left(L_0 - \frac{2L_0}{\pi} \right) \tag{5.1}$$

$$L_e = L_1 + L_2 - L_0 \tag{5.2}$$

We found the maximum folding angle ϕ_{max} to be:

$$\phi_{max} = \pi - \psi_{max} = \pi - cos^{-1} \left(\frac{L_1^2 + L_2^2 - (L_e + L_0 - x_{max})^2}{2L_1 L_2} \right) \tag{5.3}$$

Since ϕ and P has an asymptotic relationship, using δ for the minimum pressure that can prime the system, we assume that:

$$\phi = \phi_{max} \left(1 - e^{-b(P-\delta)} \right) \tag{5.4}$$

where we want to find b by using P_1 and its angle ϕ_1. In chapter 2, we have introduced equation to find force F_a and length L_a of a multi-unit linear mode pouch upon inflation [26].

$$F_a = L_o DP cos(\theta)/\theta \tag{5.5}$$

$$L_a = L_o sin(\theta)/\theta \tag{5.6}$$

We approximate a polynomial equation as in equation 5.6. It is within $0.032L_0$ difference if angle θ is between 0 and $\pi/2$. The model therefore is valid for any degrees of pouch inflation.

$$x = L_o(1 - sin(\theta)/\theta) \approx 0.16 L_0 \theta^2 \tag{5.7}$$

$$\phi_1 = 0.63\phi_{max} \tag{5.8}$$

$$L_3 = \sqrt{L_1^2 + L_2^2 - 2L_1 L_2 cos(\pi - \phi_1)} \tag{5.9}$$

$$x_1 = L_1 + L_2 - L_3 \tag{5.10}$$

As mentioned above, in this modified hinge we assume energy produced from pouch motor are all used to bend the flexure layer. The energy produced from the pouch:

$$E_a = \int_0^{x_1} F dx \tag{5.11}$$

$$E_a = \int_0^{x_1} L_0 DP \frac{cos(\frac{2.5}{\sqrt{L_0}}\sqrt{x})}{\frac{2.5}{\sqrt{L_0}}\sqrt{x}} dx \tag{5.12}$$

$$E_a = L_0 DP \frac{2sin\left(\frac{2.5}{\sqrt{L_0}}\sqrt{x_1}\right)}{6.25 L_0} \tag{5.13}$$

The energy used on the flexure:

$$E_s = \frac{\phi^2 EI}{2L_s} \tag{5.14}$$

P_1 and b can be found that:

$$P_1 = \frac{6.25\phi_1^2 EI}{4L_s D sin\left(\frac{2.5\sqrt{x_1}}{\sqrt{L_0}}\right)} \tag{5.15}$$

$$b = \frac{1}{P_1 - \delta} \tag{5.16}$$

5.1.2 Model validation

We made a pouch actuated hinge with the proposed multi-unit pouch motor as shown in Fig. 5-1 and 5-2. To validate our model, we actuate pouches and at the same time record pressure and bending angle with a pressure sensor and a camera. The same experiment is run six times and the data are plotted with a line produced from our theoretical model, as shown in Fig. 5-4. The parameters used for the theoretical line is listed in the table 5.1. The solid black line shows the average readings from the six experiments, and the shaded region shows its standard deviation. The dotted line shows the theoretical model.

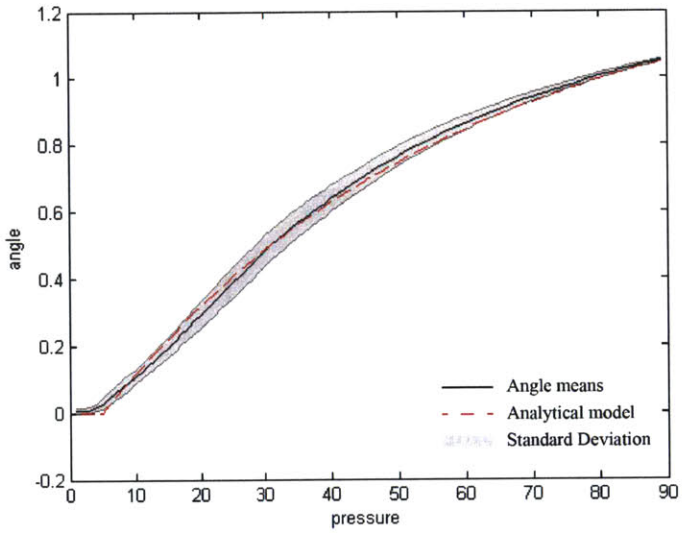

Figure 5-4: Predicted hinge angles and the average of measured hinge angles were plotted with respect to pressure. The shaded area represents standard deviation.

Table 5.1: Values used in analytical model of hinge angle

Resting Actuator Length	R_0	31 mm
Attachment length 1	L_1	11.6 mm
Attachment length 2	t_p	25.7 mm
Spring length	L_s	0.12 mm
Spring thickness	t_s	0.25 mm
Hinge stiffness	E	3 GPa
Hinge width	D	23.5 mm
Shape factor	ε	0.6
Priming pressure	δ	5 kPa

5.2 Applications

5.2.1 Non-Controlled Folding: Dodecahedron

In the first application, a dodecahedron, we demonstrate how the simplest pneumatic self-folding can be achieved and maintained with a valve, and how it can be unfolded.

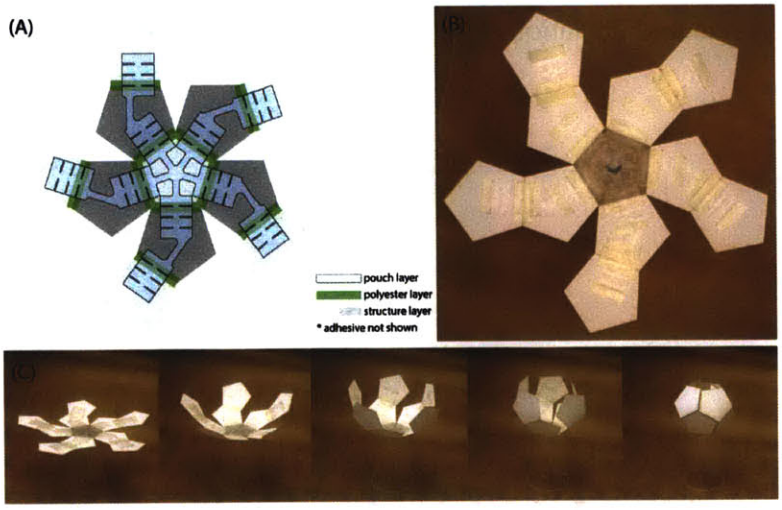

Figure 5-5: A self-fold dodecahedron. (A) 2D design (B) automatically fabricated dodecahedron (C) dodecahedron self-folding process

Using a laser cutter, we first cut out eleven pentagons, one of which is from a 1/16 inch thick acrylic sheet material, and the other ten are from a 20 mil thick cardboard. They are taped together with polyester flexure. The acrylic pentagon is placed at the center, because it is heavier and helps the structure to stand in place throughout pouch inflation.

The cardboard pieces are lightweight, making torque required to lift them almost negligible.

Using an air compressor and with some pressure regulations, a stream of 90kPa compressed air is sent into the pouches through a one-way valve, which takes about 33 seconds to inflate and completely folds the dodecahedron shape.

The one-way valve is effective to maintain the shape of the folded dodecahedron for only about 4 hours. No obvious leaks were observed, but they are likely to take place at the tubbing connections, because we found those connectors detach easily at inflation. Using the one-way valve makes the unfolding a manual process. One needs to unplug the valve to unfold. Once the valve is unplugged, it takes about 2 seconds for the dodecahedron to unfold to about 80% flat. TO fully automate unfolding, this valve needs to be replaced with an electrical one.

5.2.2 Fold and Actuation on a Gripper

In the second application, a robotic gripper, we demonstrate how pouch motors can refold folded joints, making a robot reconfigurable with open-loop pressure commands: A stand folds up to support the base of the gripper, and then gripper elbow will be controlled to fold to desired angles. Finally fingers on the gripper will be actuated to grab a lightweight object.

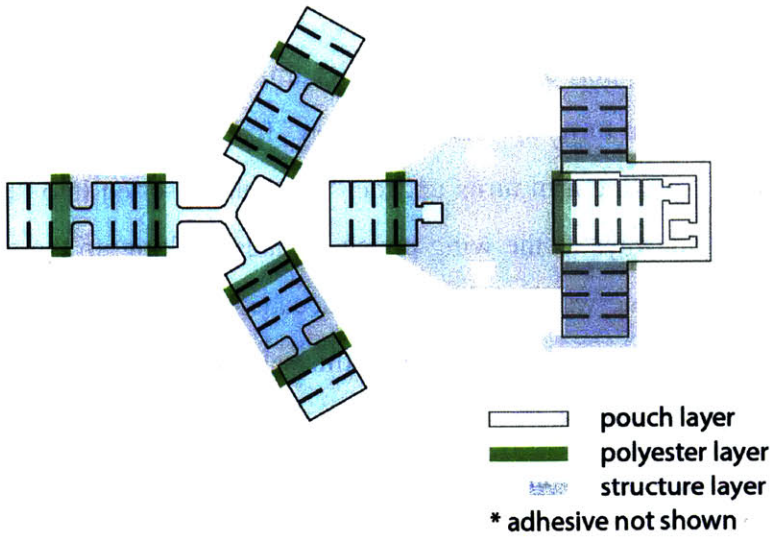

Figure 5-6: Self-folding Gripper 2D design

We choose to use lightweight 1/16 inch thick acrylic sheet material to make the parts below gripper elbow, and 20 mils cardboard material to make the parts above the gripper elbow. Because different parts fold to both directions, there are two pouch motor layers one applied to the top and the other on the bottom of the structural layer. In addition, to demonstrate a novel self-locking mechanism, this time we fold up the gripper step-by-step, instead of folding all joints together.

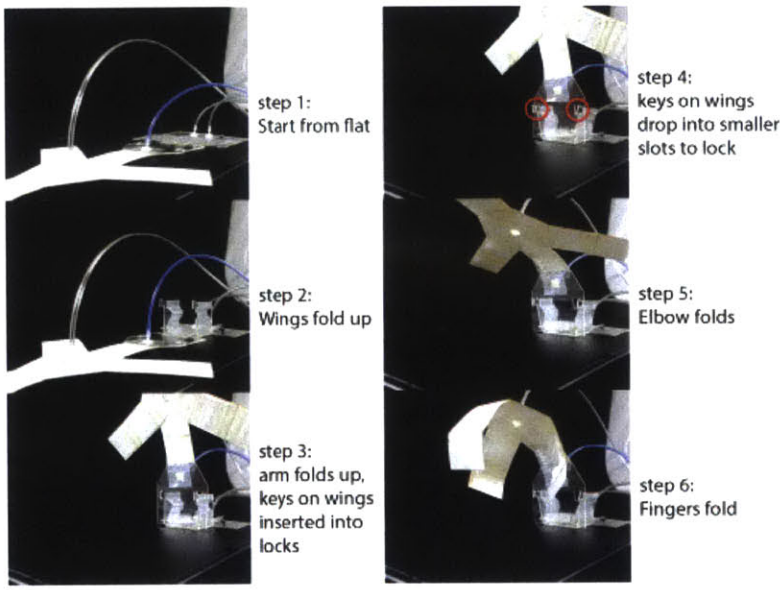

Figure 5-7: Gripper sequential folding process. Steps 2-4 illustrate the self-locking mechanism used

Fig. 5-7 explains how this gripper folds up. The first step of folding utilizes a self-locking mechanism to support the gripper with its arm. Two wings on the base are actuated to fold first. Then the arm turns up. There is a "key" feature on each wing and two "locks" features on the arm. As the arm turns up, the "keys" are inserted into "locks". Then the "keys" are pushed sideways as the wing pouch deflates, locking up the arm piece. Compared to the fold using one-way valve on the dodecahedron, because no air pressure needs to be maintained to support the arm fold with this self-lock, this fold can be permanent if keys are not actuated to unlock.

We demonstrate pressure controlled folding at the elbow as the second step of folding the gripper. The pressure of the elbow pouch is controlled with a pressure feedback loop using an Arduino microprocessor by opening and closing the air supply and exhaust valves.

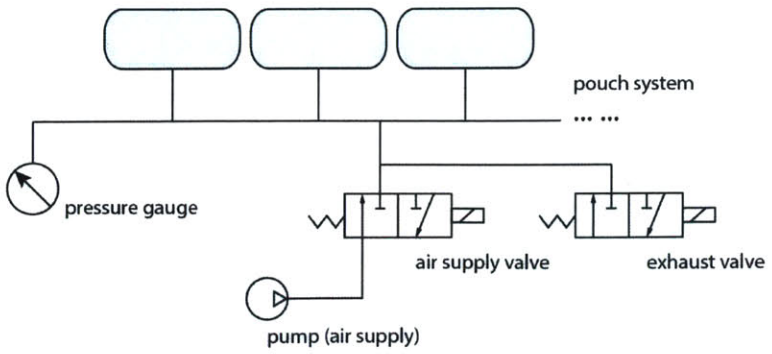

Figure 5-8: Pressure control system designed to manipulate folding angle

Although we have developed an analytical model, using pressure to predict the folding angle, we found that the geometry of the joint and gravity still leaves an non-negligible effect in applications. Therefore, to better control the elbow joint, we pursued a empirical approach. We first characterize the "elbow hinge pressure to folding angle" relationship with experiments. Then we use this experimental data to form a third power polynomial formula. In the demonstration, we plugged it back into the control algorithm to control elbow and evaluate its performance.

At 0kPa, we observed a folding angle caused by the weight of the "hand". Each subsequent command was taken after the previous command. As a result, we observed the average error to be 0.75 degrees.

5.3 Discussion

In this chapter, a pneumatic technique to fold robotic structures and machines has been studied. This novel technique has advantageous features over other types of self-folding. It is dynamic, making it applicable to fold solar panels dynamically with sun location. It is reversible and repeatable, making it applicable for household robots that can fold up itself for house cleaning and unfold itself for storage.

Pouch motor actuated self-folding also has limitations. More powerful miniature pumps and methods to adhere pouch to structural layers are needed as the structure becomes heavier weighted. Pouch designs to fold even larger folding angles also need to be developed to form more complex folded geometry. In addition, pneumatic control system becomes

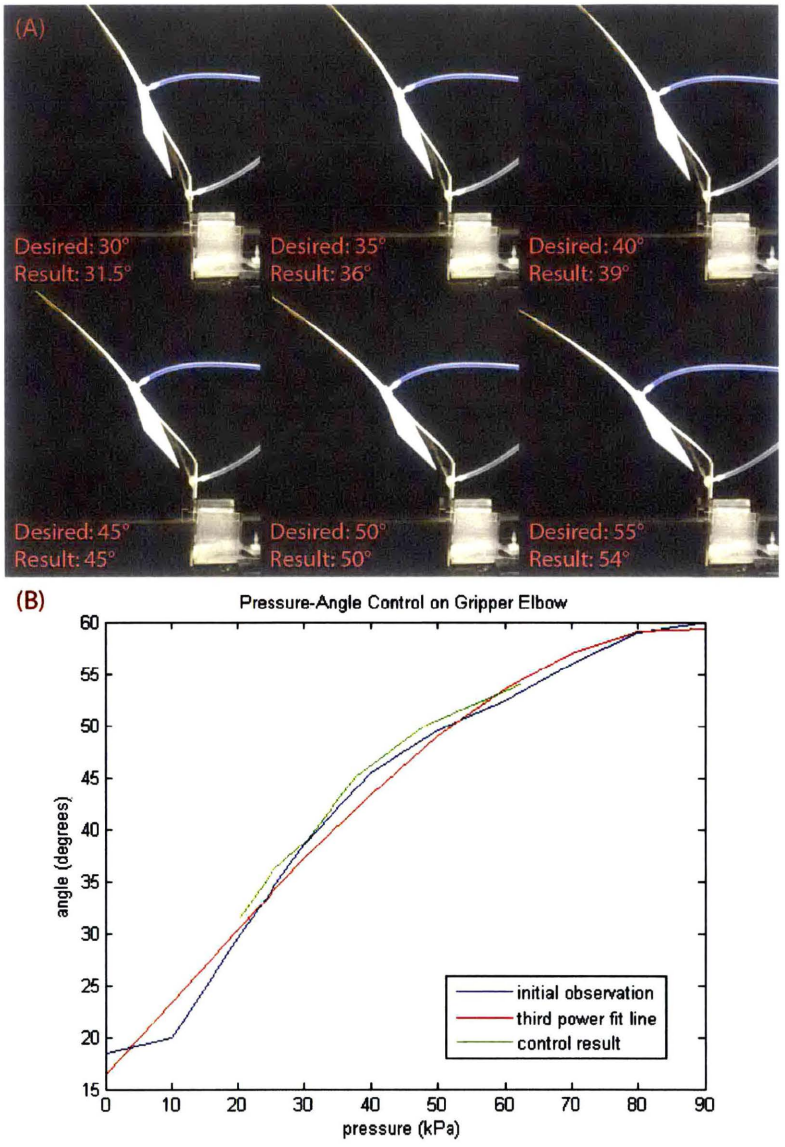

Figure 5-9: pressure-angle bending control on elbow (A) commanded bending results (B) a plot of comparison of the observed raw data, a third power fit line, and the commanded bending results

rather complex with increasing steps of folding pouches. Methods that use small number of valves for multiple pneumatic units have been explored [25], but integration to pouch motor system still needs to be done.

Table 5.2: Comparison of Self-folding methods

Actuation	Hinge length	Reversible?	Max angle	fold time
Pre-Stress [19] [22]	10 μm	Yes	135°	100 ms
SMA [14]	1 cm	Yes	180°	10 s
SMP [10] [8]	1 cm	No	135°	60 s
Pneumatics	1 cm	Yes	90°	1 s

We summarize other self-folding methods with a matrix including hinge length, reversibility, maximum folding angle and folding time in table 5.2. Besides, pouch motor actuated self-folding is also easier to make compare to SMA hinges. SMA folding angles need to be carefully designed and installed by mechanical stops, significantly making it more complex and time consuming to make.

Chapter 6

Applications in Human Computer Interaction

Pouch motors are soft and lightweight. Their shapes can be customized with our flexible thermal drawing process. These characteristics making it suitable not only to actuate origami-like robotic structures but also for everyday objects.

In this chapter, we extend our work on robotic pouch motor applications to HCI domain. We created two types of pouches with a sticky back, called "sticker" and "tape" actuators. We use them to generate linear, angular or combined motions on everyday objects including origami, toy, drawer, box and a lamp. We developed a new control system that can record and playback pouch motor inflation events, making it well-suited for HCI projects. Lastly, we conducted a user study to teach children how to use pouch motors to animate motions on origami, and their feedback are collected.

This chapter is based on our work published in [28].

6.1 Sticker Design

We use thermal drawing fabrication to make sticker and tape actuators because of its flexibility. At the end of making pouches, we put on a sticky back on those pouches with double sided tape.

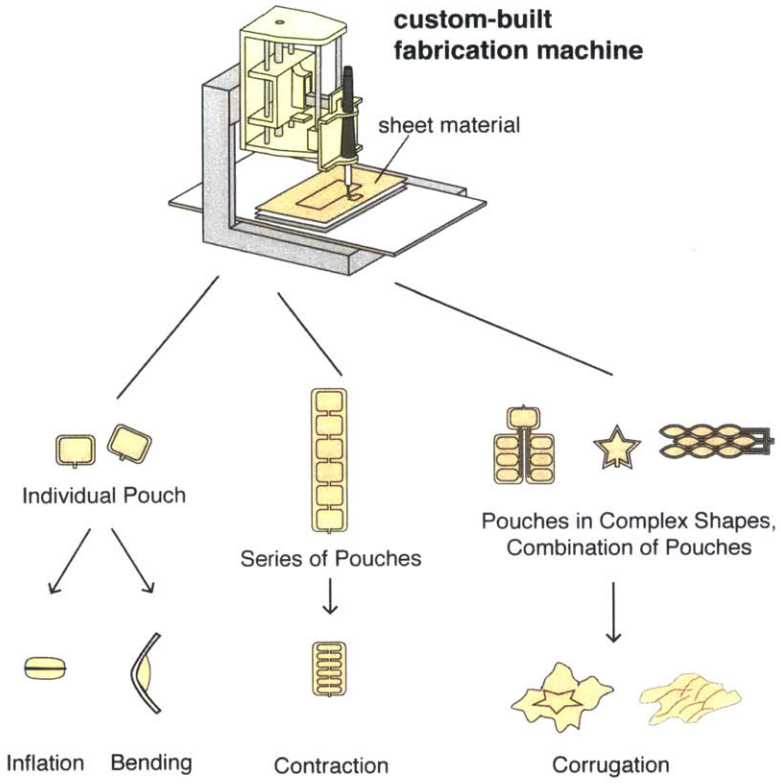

Figure 6-1: Overview of the sticky actuator family

6.1.1 Tape Actuator

Tape actuators are stored as a rolled tape form. User can cut out any length with scissor or by tearing, and conveniently put it on to an object to generate motion. The model used in this chapter are made with 4 mil thick PE films. Each printed pouch unit is 24mm long and 50mm wide.

A piece of tape actuator is effectively the classical linear mode pouch motor as introduced in chapter 2 but with added adhesive back. It shrinks in length at inflation, introducing motion on the actuated object.

6.1.2 Sticker Actuator

Sticker actuator is a single unit angular mode pouch motor as introduced in chapter 2 with added adhesive back. In this chapter, we not only use the angular mode actuation introduced from its curved surface at inflation, but also use its growth in height for a "pushing" motion.

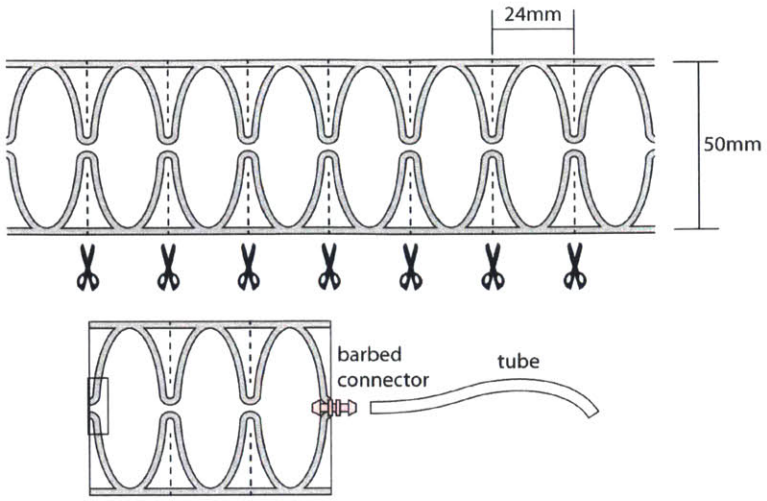

Figure 6-2: Design of the tape actuator (top), and an sample of three pouches tape actuator with connector (bottom)

Like tape actuator user simply peer off a sticker from the substrate and apply it onto a target object to generate motion.

The model used in this chapter is made with 2 mil nylon films. They are 28mm long and 10mm wide rectangles.

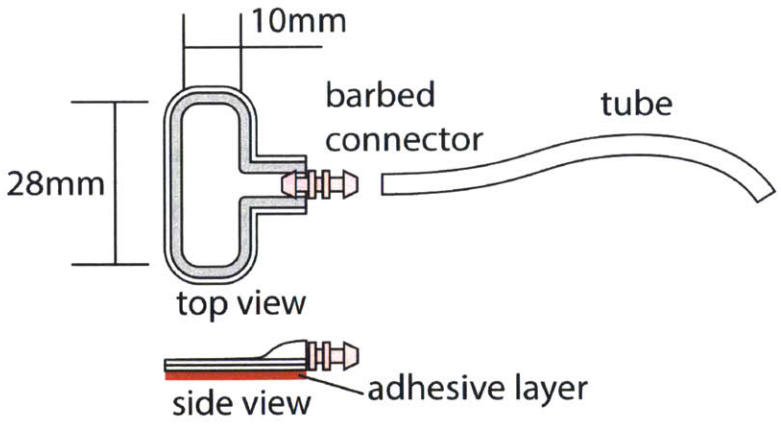

Figure 6-3: Design of the square-shape sticker actuator

6.2 Control

6.2.1 Manual Control

For casual uses, we recommend a manual inflation technique with a syringe. Users can simply pump air with the syringe to pouches. Syringes are convenient to store and intuitive to operate.

6.2.2 Programmable Control: Teaching-Playback

We have developed a programmable pneumatic control system with air supply and exhaust valves in earlier applications. By adding a teaching-playback function, we modified it to be a playing controller. With the record button on the side pushed down while operating, the operations can be recorded and playback later once the record button is released. The recorded inflation sequence can be erased by quick clicks. With this easy-to-use controller, users are able to animate motions with pouch motors without any prior programing experience.

6.3 Application Examples

To demonstrate the versatility of both tape and sticker actuators, we applied them on a variety of every day objects, including opening boxes, adjusting a desk lamp, opening and closing a drawer, animating origami and play doh motions, and to post-it notes. With the newly developed controller, we demonstrate how to make a robot toy dance.

6.3.1 Tape Actuator Examples

To open a box with two tapes, we simply adhere one end of a tape onto the cover and the other end on the side of the box. When they are inflated, they pull open the box.

To adjust the height of a desk lamp, we adhere two ends of a tape onto two bars of the lamp stand. When inflated, the tape pulls down the lamp head, making it closer to the desk.

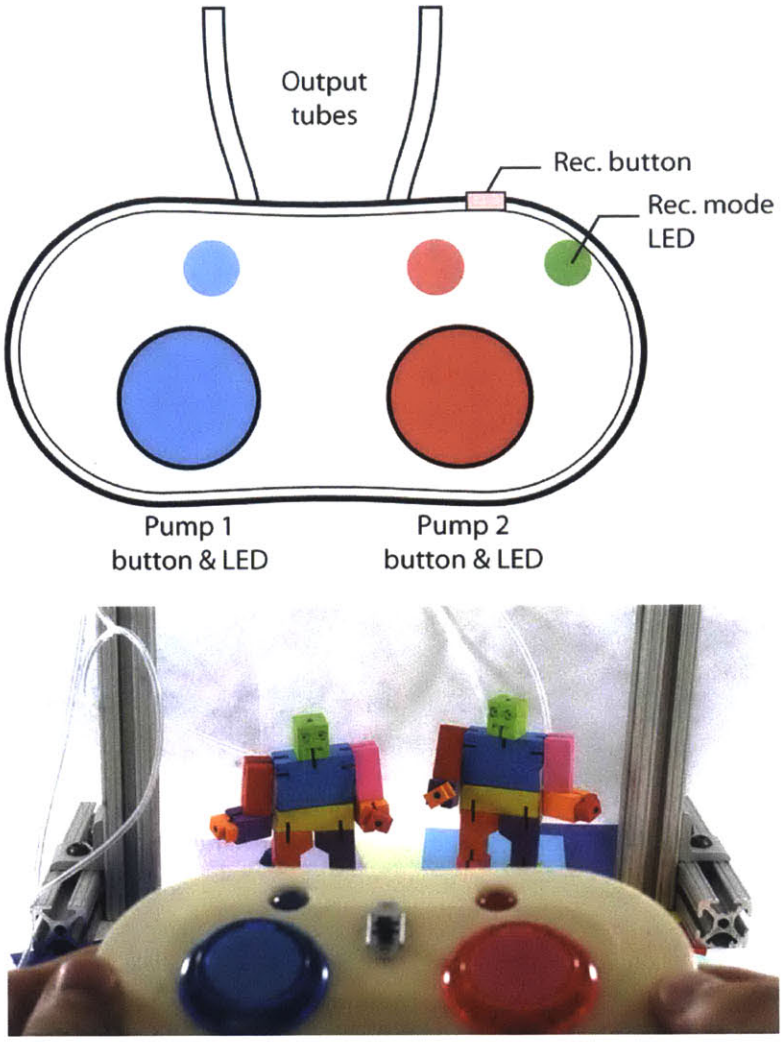

Figure 6-4: Design of the teaching-playback controller

To close a drawer, we adhere one end of a tape onto the drawer and the other end onto the its case. When inflated, it pulls the back of the drawer to close.

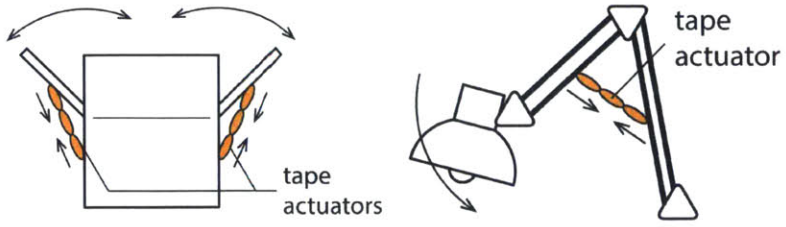

Figure 6-5: Applied tape actuators on the everyday objects: paper box (left) and desk lamp (right)

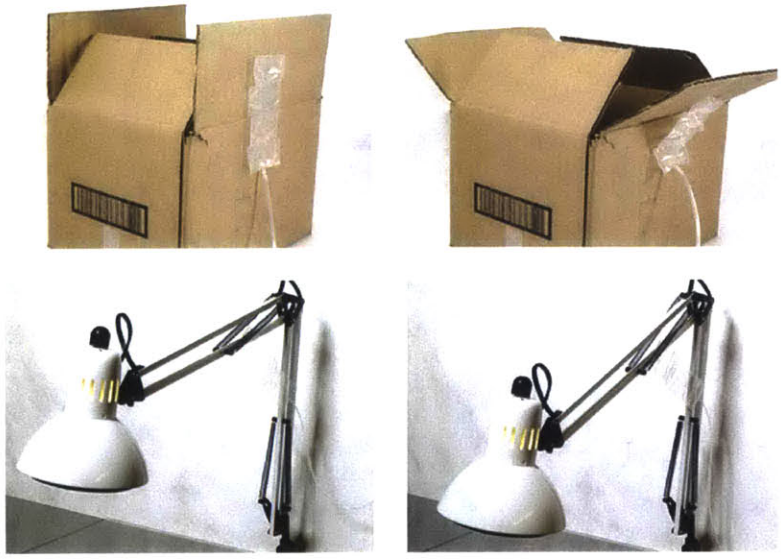

Figure 6-6: The snapshots of the movements: open/close the paper box (top), and swinging the lamp arm (bottom)

6.3.2 Sticker Actuator Examples

We applied two sticker actuators onto the bottom of an origami crane. With series of inflation and deflation of two pouches at the same time, crane flaps its wings.

We applied two sticker actuators onto two sides of an origami fish. By inflating and deflating them one after another, the fish waves its tail.

Both origami examples utilize the angular mode actuation. However, the motions animated are not just limited to angular mode. We insert a sticker into the mouth of a frog

Figure 6-7: Top: drawer open. Bottom: drawer closed after tape inflated

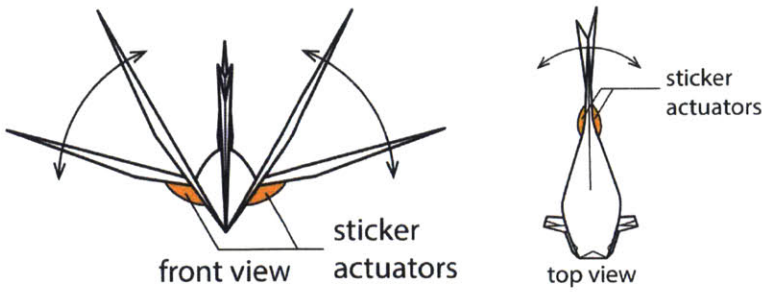

Figure 6-8: Applied sticker actuators on the origami objects: origami crane (left) and origami fish (right)

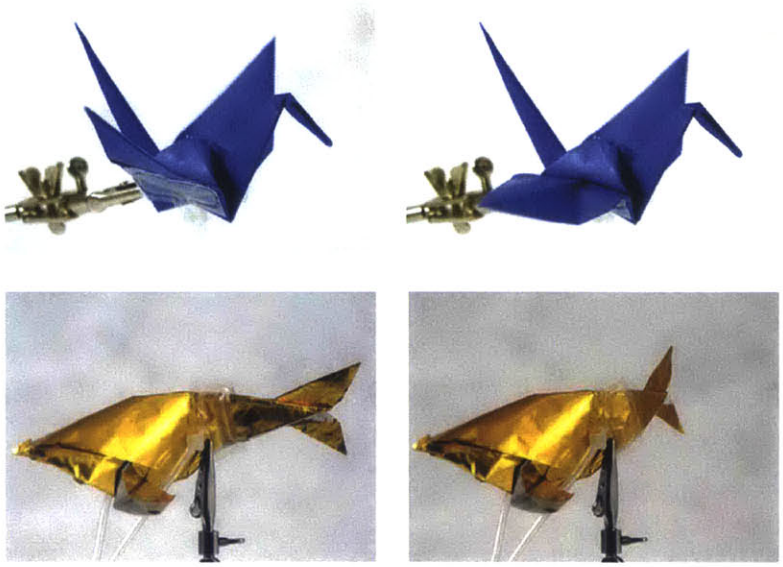

Figure 6-9: The snapshots of the movements: flapping wings (top), and swinging the tail fin (bottom)

made with play-doh. By inflating and deflating, this time the pouch uses the change in height to pushes up and down frog mouth, making it to croak.

On a post-it note, we put on the sticker actuator on the back. By inflating and deflating, the curving of the pouch surface corrugates the post-it note surface. This motion can easily catch viewers attention, making the content of the post-it note more eye-catching.

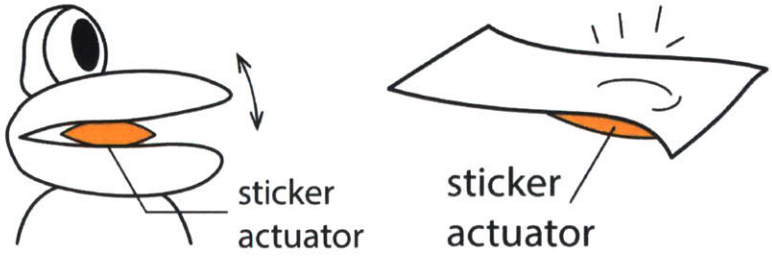

Figure 6-10: Applied sticker actuators on play dough objects (left) and sticky note (right)

6.3.3 Mixed Example

We stagged a dancing play with a toy robot. We attached sticker actuators under its arms, which makes it to raise arms with inflation. We also attached a tape actuator hanging it to a frame, which makes it to jump up and down. This time we used the new controller to

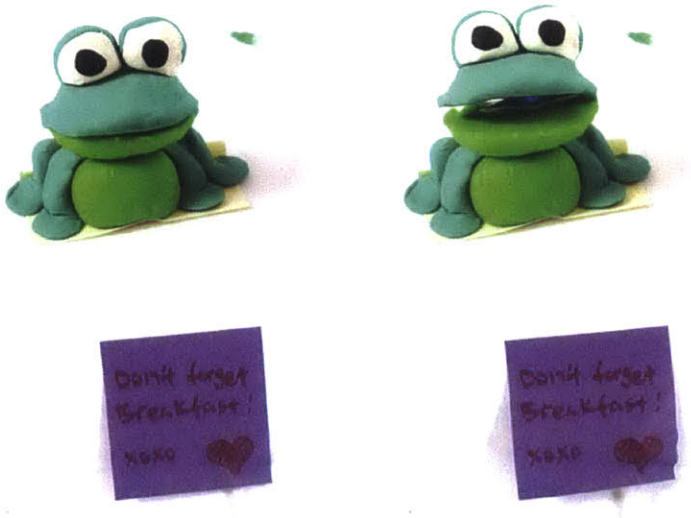

Figure 6-11: The snapshots of the movements: singing clay frog (top), and beating sticky note (bottom)

record and playback the dance.

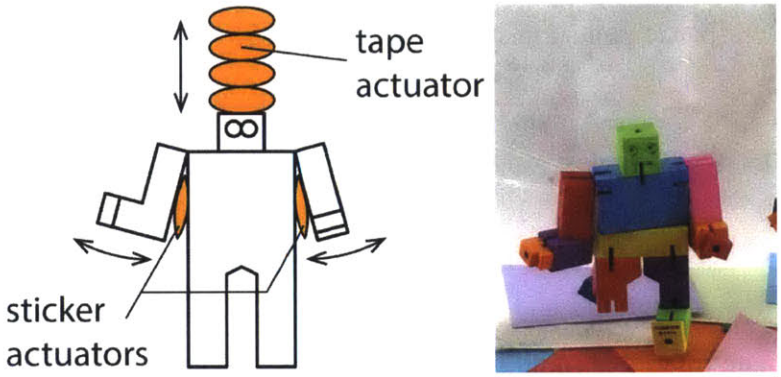

Figure 6-12: The example that use multiple sticky actuators: actuator arrangement (left), initial state (right)

6.4 User Study

6.4.1 Basic Setup and Participants

To explore how the sticker and tape actuators can be used by others, we conducted two 90-minutes workshops. Twenty kids and their parents were invited in each session. We

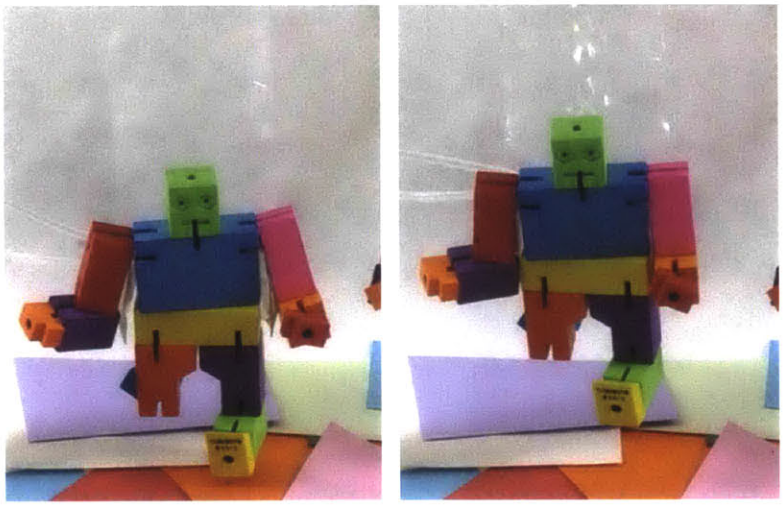

Figure 6-13: The actuators is used for dancing and jumping motion: arm swing with sticker actuators (left), and jumping with tape actuator (right)

fist teach how to fold various origamis and how the origamis can be animated with sticker actuators, and then ask the participants to create their own. We collected our findings with a short survey.

The age of our participants are shown in figure 6-15.

6.4.2 Workshop Findings

We found that as large as 70% of the sticker uses were to animate origami animal motions, including flapping, swimming and walking. Interestingly, although the sticker actuator is capable to animate rotational motions, linear motions and the combination of both, 95% of the creations from the workshop were animated in rotational motions. This indicates that angular mode actuation is the most intuitive animation with pouch motors.

Folding origamis were easier for older and more experienced participants. The most difficult task in the workshop appears to be where to attach sticker actuators to animate proper motions. Origami crane was very popular amount all creations. They were all actuated with sticker actuators to flap wings, although locations of where to adhere sticker were not always on the bottom of the wings.

In the survey, some of the questions we asked are: (1) "What did you make today?" (2) "How did you use the pouch motor?" (3) "Please let us know if you have any other

Figure 6-14: The animated origami workshop

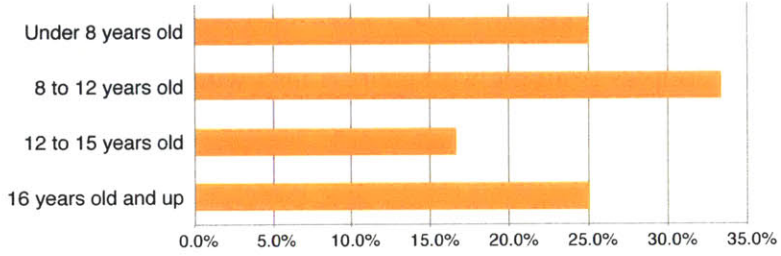

Figure 6-15: The age of the participants

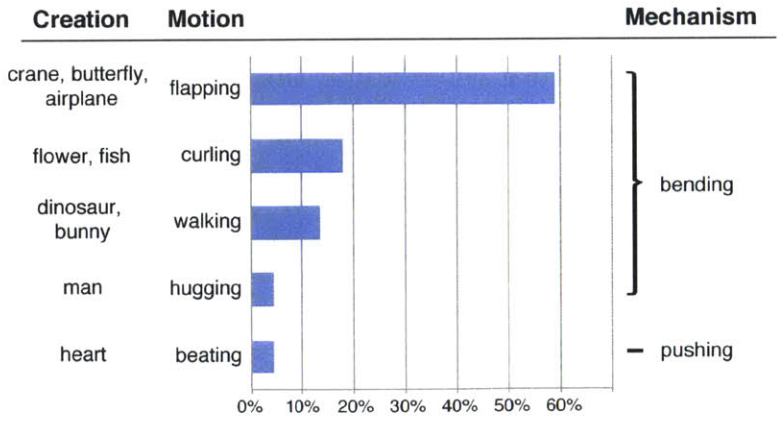

Figure 6-16: The analysis of motions and mechanisms of the results

questions, comments, or requests." We collected some very inspiring responses. One respondent commented that actuating motion was challenging: "The actuator was very interesting, and depending on the origami, there were different challenges" Someone else praised sticker actuation to be a new dimension of love: "I definitely enjoyed it. It added a new dimension to an art I love".

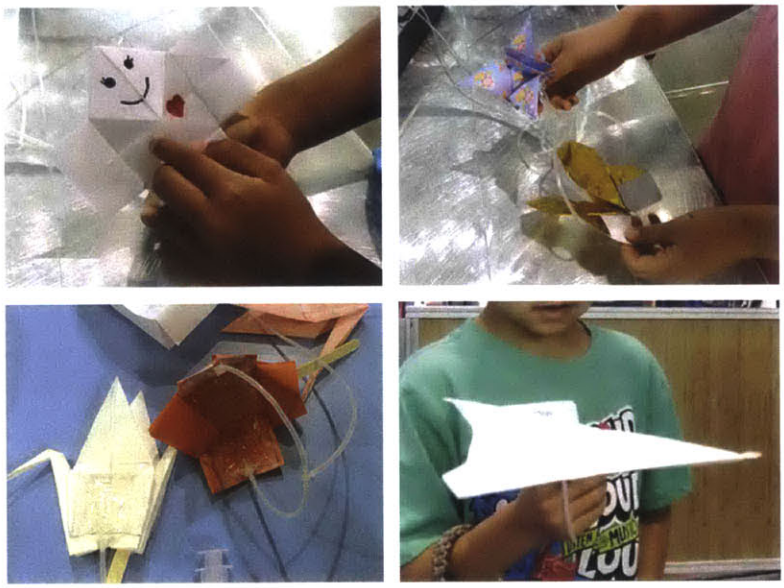

Figure 6-17: The examples from the workshop: a man with heart beat, a blooming flower with a flapping butterfly, a flapping crane, a hugging man, and an airplane with flaps

6.5 Discussion

In this chapter, sticker and tape actuators are introduced for HCI applications. They are pouch motor with special forms that can be readily attached to everyday objects to animate motions. Several examples are presented with both manual (syringe) and programmed (playback) control. User studies are conducted and responses are recorded. It is found that tape and sticker actuators are easy to use and understand and helps to express motions in art.

Chapter 7

Other pouch motor application examples

Several pouch motor enabled robotic applications are presented in previous chapters. In this chapter, I will review more pouch motor applications to show the versatility of this new printable robotic technology. The legged robot example from [26] shows that a pouch motor system can be compact to fit on a small robot. The robot hand from [27] explores different designs using co-design algorithm on the same application. The robot garden project from [30] presents a large pneumatic control network actuating a variety of customized pouch motor driven flowers.

7.1 Legged Robot: pouch motor in small robot systems

The legged quadruped robot [26] shown in Fig 7-1(left) is folded up from a piece of cardboard. By alternately inflating two angular mode pouch motors at the front and back of the body, the robot is propelled to move forward. Leg-to-body joints are rigid and not involved in this mechanism.

Depends on pressure needs, although in applications in previous chapters most of them are tethered and enabled by an air compressor capable of providing stable pressure as big as 40kPa, some small pouch motor actuated robotic applications only requires a fraction of that pressure. This legged robot, for example, uses miniature pumps that can pump to about 4kPa. As the pump size decreases, all components can be carried on the robotic structure (Fig. 7-1(right)). In this case the robot is only 70mm tall and 125mm long.

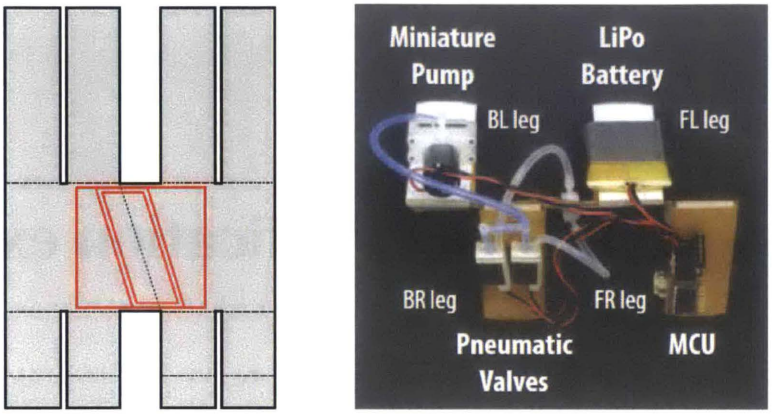

Figure 7-1: Left: Walking robot fold pattern. Angular mode pouch motors are positioned in the red squares. Right: Top view of folded walking robot. [26]

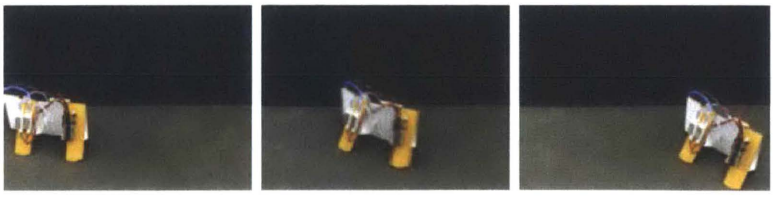

Figure 7-2: The robot walks from left to right. Here are three frames taken during the walking motion, with the left one been the first shot, right one been the second shot and third one been the third shot. [26]

7.2 Robot Hand: exploring different designs with the same application

In chapter 3, a computer-aided co-design algorithm is discussed. A flat robot hand mimicking a human hand grasping motion [27] is designed a on a cardboard and can be actuated by pouch motors at hinge joints. The co-design algorithm is used to produce four different pouch systems. The pouch locations are the same (at joint locations) in all cases, but the position of the input ports varies. Pouches are also grouped differently. The final air channel routing are generated as expected.

All four examples are fabricated using the heat drawing method. It takes about 10 minutes to fabricate for one hand. We also developed a pneumatic control system When the pressure is at 40kPa, pouch motors produce 0.5N on each finger. It can bend fingers to 90° at about 80kPa, and is capable to grab objects.

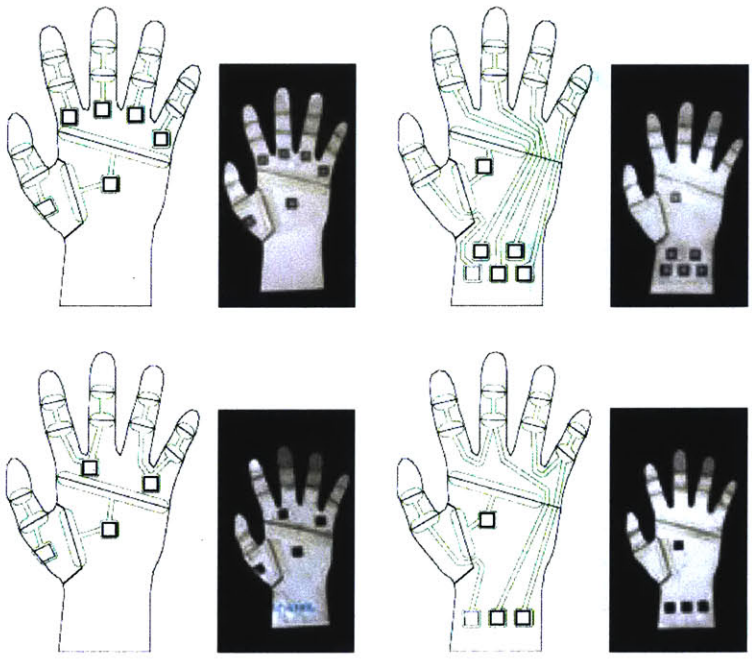

Figure 7-3: Robot Hands with four different pouch routing configurations [27]

7.3 Robot Garden: pouch customization and pneumatic control network

The Robot Garden project [30] was developed as an education outreach tool to teach high-schoolers programming. Because pouch motors are customizable and can be hided with origami, it is used to actuate the blooming motions of origami flower petals.

Novel pouches are designed for 8 different types of flowers. There are 100 flowers in total in the garden. Actuating them by a programmed Bluetooth coordination becomes a nontrivial task.

Figure 7-4: An overview of the Robot Garden [30]

7.3.1 Pouch motor actuated flowers

Eight types of flowers are designed for the garden project. Seven of them were origamis and one LED flower made with thin acrylic sheets. Pouch patterns are all custom-made based on the flower design and conceived blooming motions, as shown in Fig. 7-5.

Different pouch patterns are categorized into either linear or angular mode. Some angular mode pouches are already discussed in chapter 2 (Tulip, Spiral Flower and Bird of Paradise). Other flowers using angular mode pouches are: Flower Lily and the LED flower. Flowers using linear mode pouches are: Lotus, Clematis and Fireworks Flowers.

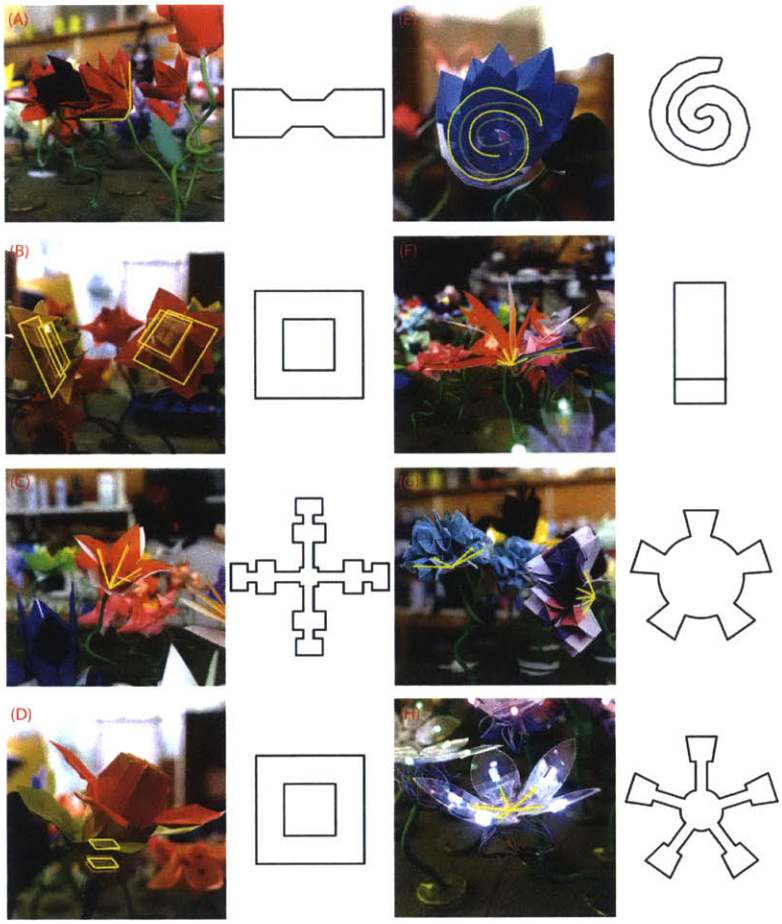

Figure 7-5: Flower and the pouch motor used are shown. The yellow line shows the location of pouches. (A)Tulip, (B) Lotus, (C) Flower Lily, (D) Clematis, (E) Spiral Flower, (F) Bird of Paradise, (G) Fireworks Flower and (H) LED Flower [30]

- Tulip: A simple dogbone shape pouch is folded halfway and laid inside petals. When inflated, it unfolds and pushes petals to open.

- Lotus: A double pouches are made using a technique shown in Fig. 2-2 and hided inside Lotus. It extends upwards with inflation to open the flower at inflation.

- Flower Lily: Although the design of the pouch looks like four stems of linear mode pouches, the pouch motor layer is actually adhered down to the flower and act like discrete angular mode single pouches for eight joints.

- Clematis: Although the 2D drawing of pouch motor is the same as the one in Lotus, two pouches are actually connected through a tubing. This allows two discrete pouches to push up and down at the same time.

- Spiral Flower: Spirals are thermally drawn on films. When inflated, it rotates making an angular mode motion. With 12 little petals adhered directly on the pouch, they appear to "twist" as the pouch inflates.

- Bird of Paradise: Multiple simple rectangular pouches are stacked but bonded on the bottom side. Petals are inserted in between two pouches. When inflated, they are separated by pouches.

- Fireworks Flower: The pouch for the Fireworks flower can be seen as five Tulip pouches connected and all hidden inside the origami. They are initially folded with the origami housing just like Tulip. The inflation moves petals to bloom.

- LED Flower: The LED flower carries several RGB LEDs on its thin acrylic petals. It uses five networked angular mode single unit pouches to actuate petal motions.

Chapter 8

Conclusions and Recommendations

8.1 Conclusions

The research in "Pouch Motor", a new family of printable soft pneumatic actuators is discussed in details in this thesis. Designed for foldable robotics, pouch motors are customizable, printed and readily integrable into robotic laminates.

Pouch motors actuation processes are studied with experimental comparisons. Coupled with a printed sensor layer, the robotic laminate composite design and fabrication processes are discussed. Feedback control, pouch motor folding and actuation in robotics and HCI are explored, and extended with other application case studies.

Compare to the introduction of pouch motors in Fall 2013 in [26], the design toolkits for pouch motor actuated robots are greatly enriched. First, pouch motors are designed with the mind of actuation mode with a variety of configurations. Second, the mathematical models capable of depicting relationships among force/torque, strain/change in angle and pressure are developed and validated through various experiments. Third, as a result from the collaboration, pouch motor network can be semi-automated generated with an algorithm [27].

The fabrication methods of pouch motors were extend from the laser bonding and stamping as seen in [26] to heat drawing, a much more robust way of making pouch motors. This enables the creation of more complicated pouch motors, such as a stacked double pouch shown in Fig. 2-2.

New ways of controlling pouch motors have also been developed. New programs were written for various applications. Most importantly, a new printable sensor layer that can be embedded in foldable robotic laminates along with a pouch motor layer was developed. Although it still has an error of about 2° and a brief delay of about 0.5s, it shows a promising direction to better control pouch motors in more complicated tasks with close-loop feedbacks.

Pouch motors were used in a lot of applications. Beside folding and unfolding foldable robots with pouch motors [34] in the robotics field, they were also used in a robot garden for programming education [30], and even in HCI to animate motions of everyday objects [28].

8.2 Recommendations

8.2.1 Current drawbacks

The sensor layer for pouch motor can be further improved by constructing a new and more complete model to better describe its behavior. Currently we have assumed a linear relationship between the bending angle and change in resistance. This approach is not sufficient to achieve more accurate control. Sensor readings drift, which is likely due to some settlement in printing fabrication.

Barbed tubbing connectors are used as an interface connecting pouch motor network with the rest of the pneumatic system. They are simply taped vy double-sided tape. As pouch inflates, the interfacing surface curves. With a high pressure, they will easily detach and leak. An alternative way would be gluing straight connectors with hot glue, which usually does not seal as good. Better ways of making the interface should be developed.

Pouch motor layer, sensor layer and structure layer are assembled together with double-sided tape. This makes the constructing process tedious. Manually aligning features on each layer is not very accurate. It also makes pouch motor behaviors less predictable as the tape is not a linear material. An automated way of constructing the robot would expedite the process and improve the pouch performance. It can be done by constructing a multi-functional CNC machine that not only makes pouch motors, but also cuts cardboards, and

adheres layers.

8.2.2 Future directions

Recently new algorithms were written to construct foldable robots from prime structures [23, 24]. It would be interesting to include pouch motor as a prime unit in the design workflow, making robotic structures generated truly fordable and not relying on electrical components.

Currently, research in pouch motor has been limited by our fabrication machine canvas size and resolution. With its customization capability, pouch motor may impact soft robotics in millimeter scale and in meter scale. Applications in different sizes can be further explored.

With an improved sensor layer, it would be interesting to explore force-feedback control. As force, pressure and position are correlated and characterized, with sensor layer monitoring the position and a pressure sensor monitoring pressure, force can be calculated and closely controlled with feedback.

Applications in pouch motors can be further explored. Wearable robotics may be an interesting area. When wearing on the body, the inflation of pouches would provide subtle haptic feedback to human body. They can also become analog controllers - as they get pressed, user can input information into the system.

Bibliography

[1] Byoungkwon An, Shuhei Miyashita, Michael T Tolley, Daniel M Aukes, Laura Meeker, Erik D Demaine, Martin L Demaine, Robert J Wood, and Daniela Rus. An end-to-end approach to making self-folded 3d surface shapes by uniform heating. In *2014 IEEE Internati Conference on Robotics and Automation (ICRA)*. IEEE, 2014.

[2] Sean A Bailey, Jorge G Cham, Mark R Cutkosky, and Robert J Full. Biomimetic robotic mechanisms via shape deposition manufacturing. In *ROBOTICS RESEARCH-INTERNATIONAL SYMPOSIUM-*, volume 9, pages 403–410, 2000.

[3] Mila Boncheva, Stefan A Andreev, L Mahadevan, Adam Winkleman, David R Reichman, Mara G Prentiss, Sue Whitesides, and George M Whitesides. Magnetic self-assembly of three-dimensional surfaces from planar sheets. *Proceedings of the National Academy of Sciences of the United States of America*, 102(11):3924–3929, 2005.

[4] Frank Daerden and Dirk Lefeber. Pneumatic artificial muscles: actuators for robotics and automation. *European journal of mechanical and environmental engineering*, 47(1):11–21, 2002.

[5] Michaël De Volder and Dominiek Reynaerts. Pneumatic and hydraulic microactuators: a review. *Journal of Micromechanics and microengineering*, 20(4):043001, 2010.

[6] Aaron M Dollar and Robert D Howe. A robust compliant grasper via shape deposition manufacturing. *Mechatronics, IEEE/ASME Transactions on*, 11(2):154–161, 2006.

[7] Saku Egawa, T Niino, and T Higuchi. Film actuators: Planar, electrostatic surface-drive actuators. In *Micro Electro Mechanical Systems, 1991, MEMS'91, Proceedings. An Investigation of Micro Structures, Sensors, Actuators, Machines and Robots. IEEE*, pages 9–14. IEEE, 1991.

[8] S Felton, M Tolley, E Demaine, D Rus, and R Wood. A method for building self-folding machines. *Science*, 345(6197):644–646, 2014.

[9] Samuel M Felton, Michael T Tolley, Cagdas D Onal, Daniela Rus, and Robert J Wood. Robot self-assembly by folding: A printed inchworm robot. In *2013 IEEE International Conference on Robotics and Automation (ICRA)*, pages 277–282. IEEE, 2013.

[10] Samuel M Felton, Michael T Tolley, ByungHyun Shin, Cagdas D Onal, Erik D Demaine, Daniela Rus, and Robert J Wood. Self-folding with shape memory composites. *Soft Matter*, 9(32):7688–7694, 2013.

[11] Samuel M Felton, Michael T Tolley, and Robert J Wood. Mechanically programmed self-folding at the millimeter scale. In *International Automation Science and Engineering (CASE)*. IEEE, 2014.

[12] Benjamin Gorissen, Michaël De Volder, Aline De Greef, and Dominiek Reynaerts. Theoretical and experimental analysis of pneumatic balloon microactuators. *Sensors and Actuators A: Physical*, 168(1):58–65, 2011.

[13] Jingjiao Guan, Hongyan He, Derek J Hansford, and L James Lee. Self-folding of three-dimensional hydrogel microstructures. *The Journal of Physical Chemistry B*, 109(49):23134–23137, 2005.

[14] Elliot Hawkes, B An, NM Benbernou, H Tanaka, S Kim, ED Demaine, D Rus, and RJ Wood. Programmable matter by folding. *Proceedings of the National Academy of Sciences of the United States of America*, 107(28):12441–12445, 2010.

[15] Aaron M Hoover and Ronald S Fearing. Fast scale prototyping for folded millirobots. In *Robotics and Automation, 2008. ICRA 2008. IEEE International Conference on*, pages 886–892. IEEE, 2008.

[16] Jack W Judy and Richard S Muller. Magnetically actuated, addressable microstructures. *Journal of Microelectromechanical Systems*, 6(3):249–256, 1997.

[17] Yoshihiro Kawahara, Steve Hodges, Benjamin S Cook, Cheng Zhang, and Gregory D Abowd. Instant inkjet circuits: lab-based inkjet printing to support rapid prototyping of ubicomp devices. In *Proceedings of the 2013 ACM international joint conference on Pervasive and ubiquitous computing*, pages 363–372. ACM, 2013.

[18] Satoshi Konishi, Fumie Kawai, and Pierre Cusin. Thin flexible end-effector using pneumatic balloon actuator. *Sensors and Actuators A: Physical*, 89(1):28–35, 2001.

[19] Kate E Laflin, Christopher J Morris, Tanziyah Muqeem, and David H Gracias. Laser triggered sequential folding of microstructures. *Applied Physics Letters*, 101(13):131901, 2012.

[20] Ying Liu, Julie K Boyles, Jan Genzer, and Michael D Dickey. Self-folding of polymer sheets using local light absorption. *Soft Matter*, 8(6):1764–1769, 2012.

[21] Yenwen Lu and Chang-Jin Kim. Characterization of balloon-jointed micro-fingers. In *ASME 2003 International Mechanical Engineering Congress and Exposition*, pages 311–316. American Society of Mechanical Engineers, 2003.

[22] Kate Malachowski, Mustapha Jamal, Qianru Jin, Beril Polat, Christopher J Morris, and David H Gracias. Self-folding single cell grippers. *Nano letters*, 14(7):4164–4170, 2014.

[23] A.M. Mehta and D. Rus. An end-to-end system for designing mechanical structures for print-and-fold robots. In *Robotics and Automation (ICRA), 2014 IEEE International Conference on*, pages 1460–1465, May 2014.

[24] Ankur M Mehta, Joseph DelPreto, Benjamin Shaya, and Daniela Rus. Cogeneration of mechanical, electrical, and software designs for printable robots from structural specifications. In *Intelligent Robots and Systems (IROS 2014), 2014 IEEE/RSJ International Conference on*, pages 2892–2897. IEEE, 2014.

[25] Nils Napp, Brandon Araki, Michael T Tolley, Radhika Nagpal, and Robert J Wood. Simple passive valves for addressable pneumatic actuation.

[26] Ryuma Niiyama, Daniela Rus, and Sangbae Kim. Pouch motors: Printable/inflatable soft actuators for robotics. In *2014 IEEE International Conference on Robotics and Automation (ICRA)*, 2014.

[27] Ryuma Niiyama, Xu Sun, Cynthia Sung, Byoungkwon An, Daniela Rus, and Sangbae Kim. Pouch motors: Printable soft actuators integrated with computational design. *Soft Robotics*.

[28] Ryuma Niiyama, Xu Sun, Lining Yao, Hiroshi Ishii, Daniela Rus, and Sangbae Kim. Sticky actuator: Free-form planar actuators for animated objects. In *Proceedings of the Ninth International Conference on Tangible, Embedded, and Embodied Interaction*, pages 77–84. ACM, 2015.

[29] D. Rus, R.J. Wood, C.D. Onal, and M. Tolley. Foldable machines, March 20 2014. US Patent App. 13/723,364.

[30] Lindsay Sanneman, Deborah Ajilo, Joseph DelPreto, Ankur Mehta, Miyashita Miyashita, Negin Abdolrahim Poorheravi, Cami Ramirez, Sehyuk Yim, Sangbae Kim, and Daniela Rus. A distributed robot garden system. submitted.

[31] ByungHyun Shin, Samuel M Felton, Michael T Tolley, and Robert J Wood. Self-assembling sensors for printable machines. In *IEEE International Conference on Robotics and Automation, Karlsruhe, Germany*, volume 31, 2014.

[32] H Sirringhaus, T Kawase, RH Friend, T Shimoda, M Inbasekaran, W Wu, and EP Woo. High-resolution inkjet printing of all-polymer transistor circuits. *Science*, 290(5499):2123–2126, 2000.

[33] Ke Sun, Teng-Sing Wei, Bok Yeop Ahn, Jung Yoon Seo, Shen J Dillon, and Jennifer A Lewis. 3d printing of interdigitated li-ion microbattery architectures. *Advanced Materials*, 25(33):4539–4543, 2013.

[34] Xu Sun, Sam Felton, Ryuma Niiyama, Robert Wood, and Sangbae Kim. Self-folding and self-actuating robots: a pneumatic approach. to appear.

[35] Xu Sun, Sam Felton, Robert Wood, and Sangbae Kim. Printing angle sensors for foldable robots. submitted.

[36] Michael T Tolley, Samuel M Felton, Shuhei Miyashita, Daniel Aukes, Daniela Rus, and Robert J Wood. Self-folding origami: shape memory composites activated by uniform heating. *Smart Materials and Structures*, 23(9):094006, 2014.

[37] Karl Willis, Eric Brockmeyer, Scott Hudson, and Ivan Poupyrev. Printed optics: 3d printing of embedded optical elements for interactive devices. In *Proceedings of the 25th annual ACM symposium on User interface software and technology*, pages 589–598. ACM, 2012.

[38] Robert J Wood, Srinath Avadhanula, Manas Menon, and Ronald S Fearing. Microrobotics using composite materials: The micromechanical flying insect thorax. In *Robotics and Automation, 2003. Proceedings. ICRA'03. IEEE International Conference on*, volume 2, pages 1842–1849. IEEE, 2003.